SPINE Volume 33, Number 1, pp 27–32
©2008, Lippincott Williams & Wilkins, Inc.

In Vivo Assessment of Lumbar Vertebral Strength in Elderly Women Using Computed Tomography-Based Nonlinear Finite Element Model

Kazuhiro Imai, MD, PhD,*† Isao Ohnishi, MD, PhD,* Seizo Yamamoto, MD, PhD,† and Kozo Nakamura, MD, PhD*

Study Design. *In vivo* study of a computed tomography (CT)-based nonlinear finite element model (FEM).

Objective. To establish an FEM with the optimum element size to assess the vertebral strength by comparing analyzed data with those obtained from mechanical testing *in vitro*, and then to assess the second lumbar (L2) vertebral strength *in vivo*.

Summary of Background Data. FEM has been reported to predict vertebral strength *in vitro*, but has not been used clinically.

Methods. Comparison among the 3 models with a different element size of 1 mm, 2 mm, and 3 mm was performed to determine which model achieved the most accurate prediction. Vertebral strength was assessed in 78 elderly Japanese women using an FEM with the optimum element size.

Results. The optimum element size was 2 mm. The L2 vertebral strength obtained with the FEM was 2154 ± 685 N, and the model could detect preexisting vertebral fracture better than measurement of bone mineral density.

Conclusion. The FEM could assess vertebral strength *in vivo*.

Key words: vertebral strength, osteoporosis, finite element model, elderly women, *in vivo* assessment. **Spine 2008;33:27–32**

Osteoporotic vertebral fractures have become a major social problem because the elderly population continues to increase. Vertebral fractures affect approximately 25% of postmenopausal women.[1] Measurement of the bone mineral density (BMD) by quantitative computed tomography (QCT) and dual energy radiograph absorptiometry (DXA) have been used to predict the risk of vertebral fracture. However, the correlation between vertebral bone strength and BMD measured by QCT is reported to be only 0.37 to 0.74,[2–7] while the correlation achieved with DXA is reported to be 0.51 to 0.80.[5–9] Therefore, such methods only explain 37% to 80% of vertebral strength. Bone strength primarily reflects the bone density and bone quality, which are influenced by bone architecture, turnover, accumulation of damage, and mineralization.[10]

It has been reported that a CT-based nonlinear finite element model (FEM) could predict vertebral strength and fracture sites accurately *in vitro*.[11] To predict quantitative strength and fracture sites is essential for the clinical application of an FEM because both parameters are important indicators of vertebral fracture risk. Prediction by an FEM with a smaller element size using the data from computed tomography (CT) scans with a thinner slice thickness and a smaller pixel size is thought to be more accurate. On the other hand, thinner CT slices lead to more radiation exposure in the clinical situation. To decrease radiation exposure as much as possible during CT scanning, optimization of the element size of the FEM was performed by assessing the accuracy of the FEM simulation.

The purposes of this study were to establish a CT-based nonlinear FEM with the optimum element size to predict the vertebral fracture load by evaluating the accuracy of our model from a comparison between predictions and data obtained by mechanical testing of human cadaver specimens *in vitro*, and then to assess lumbar vertebral strength in elderly women using the optimized CT-based nonlinear FEM.

Materials and Methods

Optimization of the Element Size of the FEM. This study used CT data and mechanical testing data obtained previously.[11] Twelve thoracolumbar vertebrae (T11, T12, and L1) with no skeletal pathology were collected within 24 hours of death from 4 men (31, 55, 67, and 83 years old). The vertebrae were disarticulated, and the discs were excised. Then the posterior element of each vertebra was removed by cutting through the pedicles. The vertebrae were immersed in water and axial CT scans with a slice thickness of 1 mm and a pixel width of 0.351 mm were obtained using a Lemage SX/E (GE Yokokawa Medical System, Tokyo, Japan) with a calibration phantom containing hydroxyapatite rods.

The 3-dimensional FEM was constructed from CT data using Mechanical Finder software (Mitsubishi Space Software Co., Tokyo, Japan). Three models with a different element size were created for each vertebra using 1 mm, 2 mm, or 3 mm tetrahedral elements. To the outer surface of the tetrahedral elements, triangular plates were attached as to form a cortical

From the *Department of Orthopaedic Surgery, School of Medicine, Tokyo University, Bunkyo-ku, Tokyo, Japan; and †Department of Orthopaedic Surgery, Tokyo Metropolitan Geriatric Medical Center, Itabashi-ku, Tokyo, Japan.

This work has been supported by the grant in aid for Scientific Research received from Japan Society for the Promotion of Science.

Acknowledgment date: March 27, 2007. Revision date: June 8, 2007. Acceptance date: July 2, 2007.

The manuscript submitted does not contain information about medical device(s)/drug(s).

No funds were received in support of this work. No benefits in any form have been or will be received from a commercial party related directly or indirectly to the subject of this manuscript.

Address correspondence and reprint requests to Isao Ohnishi, MD, PhD, Department of Orthopaedic Surgery, School of Medicine, Tokyo University, 7-3-1 Hongo, Bunkyo-ku, Tokyo 113-0033, Japan; E-mail: ohnishi-i@umin.ac.jp

Copyright © Lippincott Williams & Wilkins. Unauthorized reproduction of this article is prohibited.

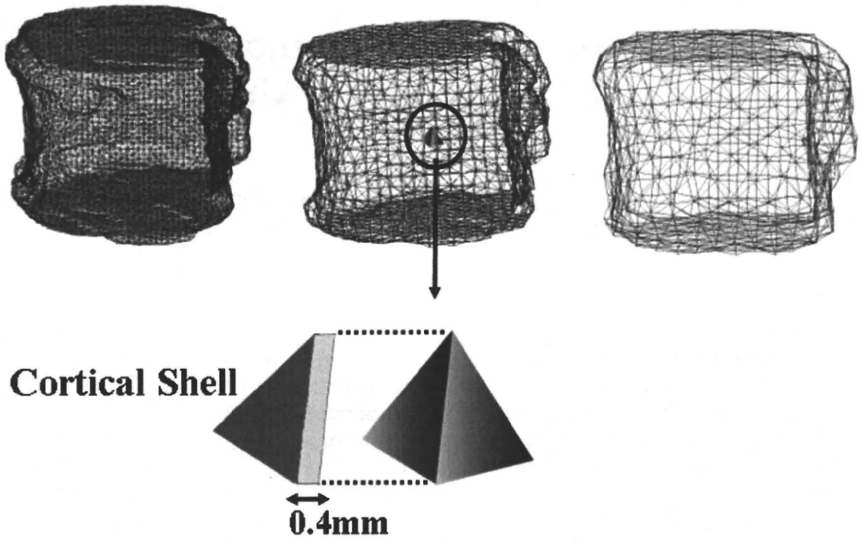

Figure 1. Finite element models of a whole vertebral body constructed with 1 mm, 2 mm, or 3 mm tetrahedral elements. The cortical shell was modeled by using triangular plates with a thickness of 0.4 mm. The model on the left consists of 104,205 nodes with 585,784 tetrahedral elements and 15,800 triangular plates constructed using 1-mm size elements. The middle model consists of 12,938 nodes with 70,022 tetrahedral elements and 3586 triangular plates constructed using 2-mm elements. The model on the right consists of 3476 nodes with 18,103 tetrahedral elements and 1330 triangular plates constructed using 3-mm size elements.

shell (Figure 1). The thickness of this shell was set as 0.4 mm based on the previous papers.[12–14]

To allow for bone heterogeneity, the mechanical properties of each element were computed from the Hounsfield unit value. Ash density of each voxel was determined from the linear regression equation created by these values of the calibration phantom. Ash density of each element was set as the average ash density of the voxels contained in one element. Young's modulus and the yield stress of each tetrahedral element were calculated from the equations proposed by Keyak *et al.*[15] Young's modulus of each triangular plate was set as 10 GPa and Poisson's ratio of each element was set as 0.4.

A uniaxial compressive load with a uniform distribution was applied on the upper surface of the vertebra and all the elements and all the nodes of the lower surface were completely restrained. Each model was analyzed using Mechanical Finder software as reported previously.[11]

A nonlinear FEM by Newton-Raphson method was used. To allow for the nonlinear phase, mechanical properties of the elements were assumed to be bilinear elastoplastic, and the isotropic hardening modulus was set as 0.05. Each element was assumed to yield when its Drucker-Prager equivalent stress reached the element yield stress. In the postyield phase, failure was defined as occurring when the minimum principal strain of an element was less than −10,000 microstrain.

The predicted fracture load was defined as the load that caused at least one element failure, while the measured fracture load was defined as the ultimate load that was achieved by mechanical testing. Pearson's correlation analysis was used to evaluate correlations between the fracture load predicted by FEM simulation and the measured fracture load. To optimize the element size of the FEM, the accuracy of prediction of the fracture load was compared among the 3 models with different element sizes. To assess the relationship between the models with a different element size, linear regression analyses were performed.

In addition, we also created models using 1.4 mm and 4.5 mm elements as well as 1 mm, 2 mm, and 3 mm elements to investigate the model convergence. For each of the models, total strain energy was calculated at a load of 1000 N, under which all specimens were in the elastic phase. Data on the total strain energy were compared among the 1 mm (average 403,033 tetrahedral elements), 1.4 mm (average 143,367 tetrahedral elements), 2 mm (average 47,687 tetrahedral elements), 3 mm (average 11,903 tetrahedral elements), and 4.5 mm (average 2719 tetrahedral elements) models.

***In Vivo* Assessment of Lumbar Vertebral Strength.** The subjects were ambulatory postmenopausal Japanese women aged 60 to 85 years. Excluded from participation were women with disorders of bone and mineral metabolism other than postmenopausal osteoporosis, those who had any recent or current treatment with the potential to alter bone turnover or bone metabolism, and those with a history of second lumbar vertebral (L2) fracture. The study protocol was approved by our ethics committee and each participant provided written informed consent. A total of 78 eligible participants were enrolled in this study.

In all the participants, the BMD (g/cm^2) of the lumbar spine (L2–L4) was measured by DXA (DPX; Lunar, Madison, WI) in the supine position and axial CT scans of L2 were obtained with a slice thickness of 2 mm and pixel width of 0.35 mm using Light Speed QX/i (GE Yokokawa Medical System, Tokyo, Japan) with a calibration phantom containing hydroxyapatite rods. The 3-dimensional FEM was constructed from the CT data using Mechanical Finder with 2 mm tetrahedral elements and 2 mm triangular plates, and the fracture load was analyzed using this software as described above.

Results are expressed as the mean ± standard deviation (SD). Statistical analysis was performed with the Mann-Whitney *U* test and the Kruskal-Wallis test. Differences were considered significant at $P < 0.05$.

■ Results

Optimization of the FEM Element Size

There was a strong linear correlation between the fracture load predicted by the FEM with 1 mm tetrahedral elements and the measured loads ($r = 0.938$, $P < 0.0001$), and the slope of the regression line was 0.934 (Figure 2A). With 2 mm elements, the correlation was even stronger ($r = 0.978$, $P < 0.0001$), and the slope of the regression line was 0.881 (Figure 2B). With 3 mm elements, the correlation was slightly weaker ($r = 0.866$, $P < 0.0001$), and the slope of the regression line was

Copyright © Lippincott Williams & Wilkins. Unauthorized reproduction of this article is prohibited.

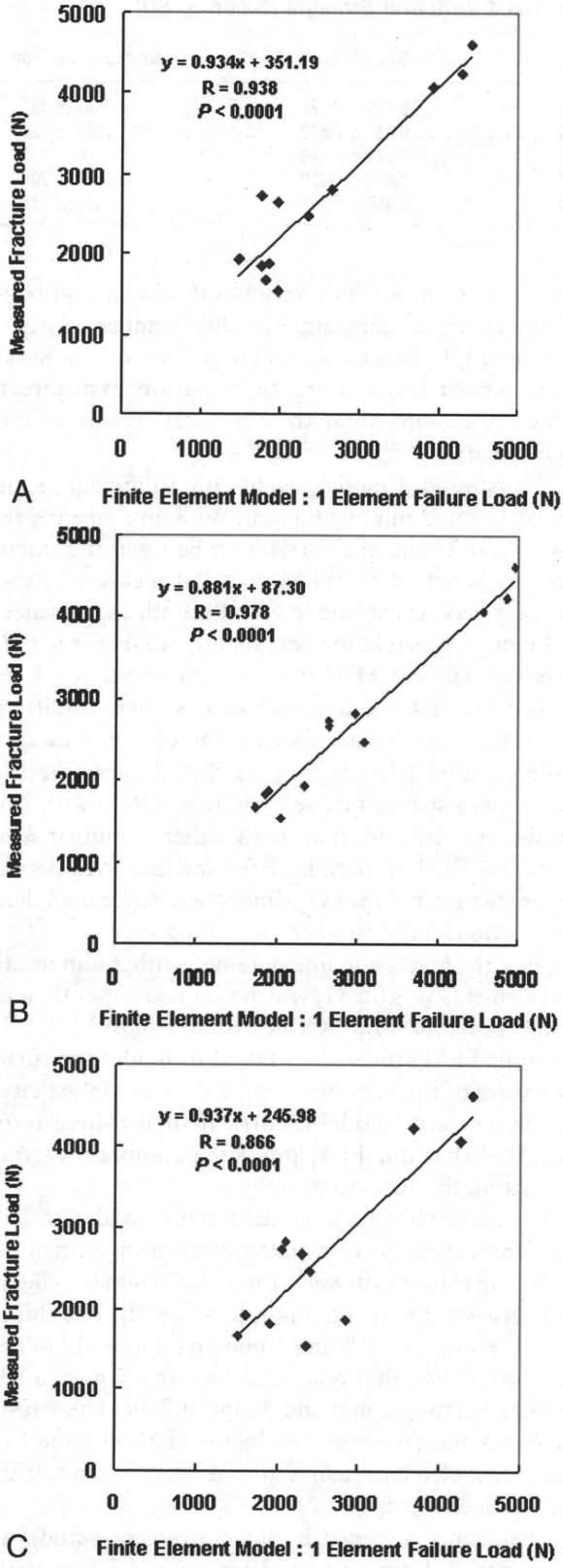

Figure 2. The measured fracture load *versus* the fracture load predicted by the finite element model (FEM). **A,** FEM with-1 mm tetrahedral elements. **B,** FEM with-2 mm tetrahedral elements. **C,** FEM with 3-mm tetrahedral elements. Strong correlations ($r > 0.90$) were obtained with elements of 1 mm and 2 mm in size, while a moderate correlation ($r = 0.866$) was obtained with 3-mm elements.

0.937 (Figure 2C). There was a strong linear correlation between the fracture load predicted by the 1 mm element model and that by the 2 mm ($r = 0.959$, $P < 0.0001$), and the slope of the regression line was 0.868. With the 1 mm and 3 mm models, the correlation was slightly weaker ($r = 0.912$, $P < 0.0001$), and the slope of the regression line was 0.839. With the 2 mm and 3 mm models, the correlation was much weaker ($r = 0.878$, $P < 0.0001$), and the slope of the regression line was 0.730.

In the convergence study, total strain energy decreased by 9.1% (4.0%–22.9%), with an increase of the element size from 1 mm to 1.4 mm. With an increase from 1.4 mm to 2 mm, it decreased by 10.0% (6.5%–17.3%), and decreased by 9.5% (2.9%–13.2%) from 2 mm to 3 mm. With an increase from 3 mm to 4.5 mm, total strain energy increased in some vertebrae although it decreased by an average of 38.6%.

In Vivo *Assessment of Lumbar Vertebral Strength*

The 78 women enrolled in the study had a mean age of 74.4 ± 5.6 years, a mean height of 148.4 ± 6.0 cm, and a mean weight of 50.3 ± 7.7 kg. The measured BMD of the lumbar spine was 0.808 ± 0.181 g/cm^2 and the strength of L2 predicted by the model was 2154 ± 685 N.

The subjects were classified into 5-year age groups, as summarized in Table 1. Height and vertebral strength showed a significant decrease in the older age groups, but weight and BMD did not change significantly (Kruskal-Wallis test, $P < 0.05$).

Next, the subjects were classified on the basis of prior vertebral fracture. Among the 78 women, 42 did not have any vertebral fractures (nonfracture group) and 36 subjects already had vertebral fractures (fracture group). Thus, vertebral fractures were present in 46.1% of the total study population. The characteristics of the 2 groups are summarized in Table 2. The nonfracture group was significantly younger than the fracture group (Mann-Whitney *U* test, $P < 0.001$). Height ($P < 0.05$) and weight ($P < 0.005$) were significantly greater in the nonfracture group than in the fracture group.

The average spinal BMD of the nonfracture group was 0.849 ± 0.146 g/cm^2, which was greater than that of the fracture group at 0.759 ± 0.207 g/cm^2 ($P < 0.05$) (Figure 3). The predicted vertebral strength of L2 was 2489 ± 580 N in the nonfracture group, which was greater than in the fracture group at 1764 ± 588 N ($P < 0.0001$) (Figure 3). The L2 strength to weight ratio was 4.80 ± 1.20 in the nonfracture group, and this was significantly greater than in the fracture group at 3.77 ± 1.36 ($P < 0.005$) (Figure 4).

■ Discussion

Assessing vertebral strength by using the FEM has been difficult because of the complex geometry, elastoplasticity, and thin cortical shell of the vertebra. The vertebrae have an elaborate architecture and geometry with curved surfaces, which cannot be modeled properly by using

Copyright © Lippincott Williams & Wilkins. Unauthorized reproduction of this article is prohibited.

Table 1. Summary of the Subjects' Height, Weight, BMD, and Analyzed Vertebral Strength (Mean ± SD)

Age (yr)	N	Height (cm)	Weight (kg)	BMD (g/cm^2)	Vertebral Strength (N)
60–64	6	153.5 ± 4.5	54.0 ± 6.1	0.850 ± 0.180	2592 ± 497
65–69	10	152.3 ± 7.8	50.9 ± 8.2	0.848 ± 0.112	2665 ± 528
70–74	21	148.1 ± 5.0	51.3 ± 7.4	0.744 ± 0.169	2050 ± 752
75–79	26	147.8 ± 6.2	48.5 ± 8.7	0.800 ± 0.200	2069 ± 706
80–85	15	145.1 ± 3.8	50.3 ± 6.3	0.867 ± 0.191	1933 ± 512

8-noded hexahedral elements. Previous mechanical tests have shown that there is a difference between the tensile and compressive strength of bone,[16–18] with compressive strength showing nonlinear behavior. Therefore, a nonlinear FEM should be used to predict the clinical fracture load. The cortical shell of each vertebra is estimated to have a thickness of approximately 0.4 mm.[12–14] In comparison, the resolution of clinically available CT scanners is fairly low, with a pixel spacing of larger than 0.25 mm. This means that the currently available CT data do not allow the thin cortical shell to be precisely modeled. The cortical thickness tends to be overestimated and its density is underestimated.[19,20] Therefore, it is necessary to construct a thinner model cortical shell from non-CT data. Shell elements of triangular plates with a uniform thickness of 0.4 mm were used to construct a cortical shell.

The characteristics of the present FEM in this study were as follows: adoption of the tetrahedral elements to model the surface curvature of the entire vertebra, utilization of nonlinear analysis to match the elastoplasticity of the vertebra during compression, and construction of a cortical shell as the surface of the model. It has been reported that the thin cortex of a vertebra contributes 12%–75% to its overall strength and the contribution of the cortex is estimated to be significantly larger in osteoporotic individuals.[21,22] Thus, the importance of the strength of the cortical shell should be taken into consideration when predicting the fracture load for osteoporosis patients.

The limitation of our model is that the cortical shell was treated as a homogenous material because the pixels of CT scans were too large to model the thin cortex. In addition, with the limited resolution of currently available CT scanners, the microarchitecture of the bone cannot be precisely assessed. Micro-CT and synchrotron micro-CT can visualize bone microstructure.[23] Therefore, an FEM based on micro-CT data may show more accurate simulation because it would be possible to model a cortical shell with heterogeneous properties and also to assess the microarchitecture. However, obtaining micro-CT scans of a whole vertebra *in vivo* would be impossible with the currently available scanners. Also, use of thinner CT slices to obtain images leads to more radiation exposure. To decrease radiation exposure for clinical use, somewhat thicker slices would be more appropriate.

Table 2. Background of the Subjects in No Fracture Group and Fracture Group

Group	N	Age (yr)	Height (cm)	Weight (kg)
No fracture group	42	72.3 ± 5.7	149.9 ± 5.7	52.6 ± 7.4
Fracture group	36	76.8 ± 4.6	146.6 ± 6.0	47.8 ± 7.3

We assessed 3 models each with a different element size of 1 mm, 2 mm, and 3 mm. With an element size of 1 mm and 2 mm, the correlation between the fracture load predicted by the FEM and that measured experimentally was very strong ($r > 0.90$). With an element size of 3 mm, the correlation was slightly weaker ($r < 0.90$). Although all of 3 FEM were generated using CT data obtained with a 1 mm slice thickness, these results suggested that the elements with a size of 1 mm or 2 mm could be used to accurately predict the fracture load. There was a stronger correlation ($r = 0.978$) with 2 mm tetrahedral elements than with either 1 mm or 3 mm elements. The correlation of the fracture load between the prediction and the experiment was better than that in the previous FEM studies ($r = 0.89–0.95$).[24–27] The slope of the regression line obtained with 2 mm tetrahedral elements was 0.881, which was also better than that in the previous FEM studies (0.569–0.86).[24–27] The previous FEM studies had failed to model the surface curvature of the vertebra, match the elastoplasticity of the vertebra, or model a cortical shell. These results indicated that our FEM predicted compressive vertebral strength more accurately.

The correlation between the fracture load with 1 mm and 2 mm elements ($r = 0.959$) was stronger than both of the correlations between 1 mm and 3 mm ($r = 0.912$), and between 2 mm and 3 mm ($r = 0.878$). The slope of the regression line relating 1 mm and 2 mm (0.868) was also better than that relating 1 mm and 3 mm (0.839), and that relating 2 mm and 3 mm (0.730). These results indicated that the prediction by the FEM with the 1 mm and 2 mm elements achieved more accurate result than the 3 mm elements.

The results obtained by the convergence study with the 1 mm, 1.4 mm, 2 mm, 3 mm, and 4.5 mm models suggested the model with 1 mm elements was the most accurate among the 5 models. However, the 2 mm model was thought to achieve sufficiently accurate prediction compared with the 1 mm model. In the previous FEM study using the models with 8-noded hexahedral elements, stiffness of the model with $3 \times 3 \times 3$ mm^3 elements was on average only 4% greater than that with

Copyright © Lippincott Williams & Wilkins. Unauthorized reproduction of this article is prohibited.

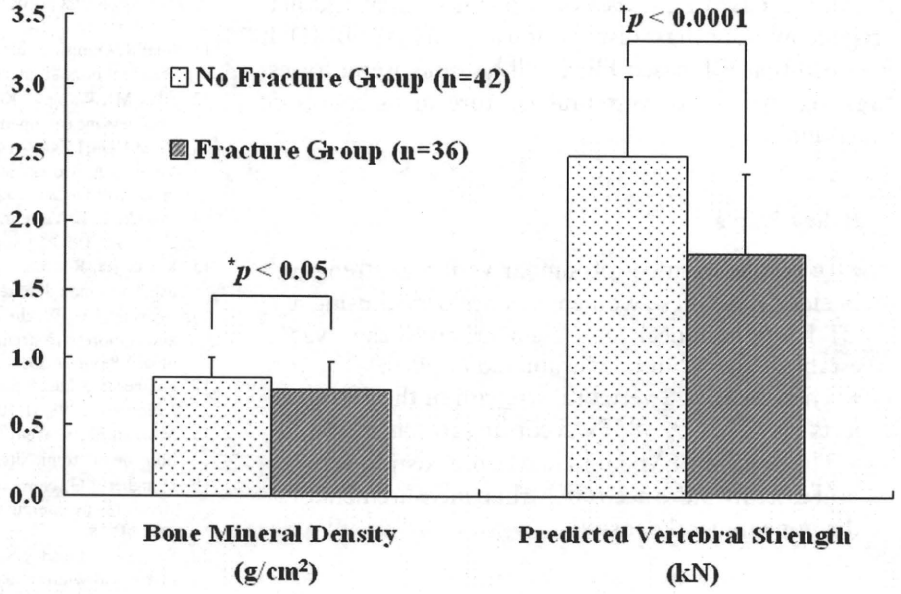

Figure 3. Bone mineral density of the lumbar spine (L2–L4) and predicted vertebral strength of the L2 vertebra in the nonfracture group (n = 42) and in the fracture group (n = 36). The error bars represent one standard deviation from the mean. Bone mineral density of the nonfracture group was greater than that of the fracture group. The difference was significant ($P < 0.05$). Predicted vertebral strength in the nonfracture group was also significantly ($P < 0.0001$) greater than that of the fracture group.

$1 \times 1 \times 1.5$ mm^3 elements, and there was a high correlation between the stiffness and the experimentally measured ultimate strength values in both $3 \times 3 \times 3$ mm^3 element model ($r^2 = 0.94$) and $1 \times 1 \times 1.5$ mm^3 element model ($r^2 = 0.92$).[28]

Based on these *in vitro* data, an *in vivo* study was performed using CT scans with a 2-mm slice thickness and a nonlinear FEM with an element size of 2 mm. There have been few reports about predicting vertebral strength *in vivo*, although some authors have assessed vertebral strength *in vitro* by mechanical testing. In the elderly, McBroom *et al* reported that among 10 specimens from subjects with an average age of 78 years, the average failure load for the L1 vertebral body was 3160 ± 424 N and it was 3385 ± 485 N for L3.[3] Eckstein *et al* reported that the average failure load for L3 was 3016 ± 149 N when they tested 102 specimens from the subjects with an average age of 80.6 years.[29] These 2 reports included both men and women. In the present study, however, all of the subjects were Japanese women. This might be one of the reasons why our predicted vertebral strength was smaller than that reported elsewhere.

The limitation in our study was that the prediction was made under a uniaxial compressive loading condition. In an *in vivo* situation, the loading and boundary conditions are completely different. However, one of the advantages of FEM simulation is that it allows us to set an arbitrary load magnitude or direction to simulate loading in various activities of daily living. If predicted strength by FEM was proved to be accurate in a uniaxial compressive loading condition, we could assume that we might be able to apply this method to predict accurately the strength under various other loading and boundary conditions. Nevertheless, the accuracy of our method in predicting strength under different loading and boundary conditions should be validated by conducting another mechanical testing and it would be one of our assignments in the future study.

In this study, the vertebral strength predicted by FEM could detect preexisting vertebral fractures better than

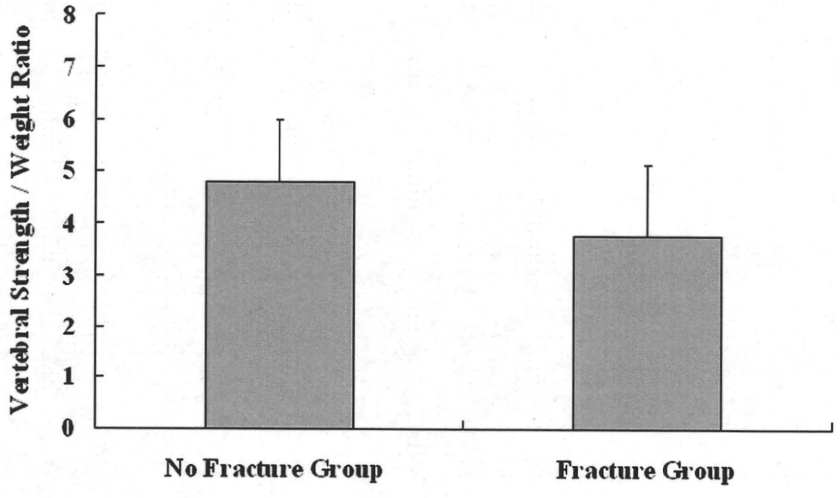

Figure 4. The ratio of L2 vertebral strength to weight in the nonfracture group (n = 42) and in the fracture group (n = 36). The difference was also significant ($P < 0.005$).

Copyright © Lippincott Williams & Wilkins. Unauthorized reproduction of this article is prohibited.

BMD. CT-based FEM assesses bone geometry and heterogeneous bone mass distribution as well as the BMD. It is hoped that CT-based FEM will become useful for estimating the risk of vertebral fracture in osteoporotic individuals.

■ Key Points

- *In vivo* assessment of lumbar vertebral strength in elderly Japanese women was performed using a CT-based nonlinear finite element model that was established and initially evaluated *in vitro*.
- The average L2 vertebral strength of the 78 subjects was 2154 ± 685 N according to this model.
- The present FEM could detect preexisting vertebral fracture more accurately than measurement of the bone mineral density.

References

1. Melton LJ. Epidemiology of spinal osteoporosis. *Spine* 1997;22(suppl):2–11.
2. Mosekilde L, Bentzen SM, Ortoft G, et al. The predictive value of quantitative computed tomography for vertebral body compressive strength and ash density. *Bone* 1989;10:465–70.
3. McBroom RJ, Hayes WC, Edwards WT, et al. Prediction of vertebral body compressive fracture using quantitative computed tomography. *J Bone Joint Surg Am* 1985;67:1206–14.
4. Brinckmann P, Biggemann M, Hilweg D, et al. Prediction of the compressive strength of human lumbar vertebrae. *Clin Biomech* 1989;4(suppl):1–27.
5. Edmondston SJ, Singer KP, Day RE, et al. In-vitro relationships between vertebral body density, size and compressive strength in the elderly thoracolumbar spine. *Clin Biomecha* 1994;9:180–6.
6. Cheng XG, Nicholson PH, Boonen S, et al. Prediction of vertebral strength in vitro by spinal bone densitometry and calcaneal ultrasound. *J Bone Miner Res* 1997;12:721–8.
7. Eriksson SA, Isberg BO, Lindgren JU. Prediction of vertebral strength by dual photon absorptiometry and quantitative computed tomography. *Calcif Tissue Int* 1989;44:243–50.
8. Myers BS, Arbogast KB, Lobaugh B, et al. Improved assessment of lumbar vertebral body strength using supine lateral dual-energy x-ray absorptiometry. *J Bone Miner Res* 1994;9:687–93.
9. Bjarnason K, Hassager C, Svendsen OL, et al. Anteroposterior and lateral spinal DXA for the assessment of vertebral body strength: comparison with hip and forearm measurement. *Osteoporosis Int* 1996;6:37–42.
10. NIH Consensus Development Panel on Osteoporosis Prevention D, and Therapy. Osteoporosis prevention, diagnosis, and therapy. *JAMA* 2001;285:785–95.
11. Imai K, Ohnishi I, Bessho M, et al. Nonlinear finite element model predicts vertebral bone strength and fracture site. *Spine* 2006;31:1789–94.
12. Silva MJ, Wang C, Keaveny TM, et al. Direct and computed tomography thickness measurements of the human, lumbar vertebral shell and endplate. *Bone* 1994;15:409–14.
13. Vesterby A, Mosekilde L, Gundersen HJ, et al. Biologically meaningful determinants of the in vitro strength of lumbar vertebrae. *Bone* 1991;12:219–24.
14. Mosekilde L. Vertebral structure and strength in vivo and in vitro. *Calcif Tissue Int* 1993;53(suppl):121–6.
15. Keyak JH, Rossi SA, Jones KA, et al. Prediction of femoral fracture load using automated finite element modeling. *J Biomech* 1998;31:125–33.
16. Keaveny TM, Wachtel EF, Ford CM, et al. Differences between the tensile and compressive strengths of bovine tibial trabecular bone depend on modulus. *J Biomech* 1994;27:1137–46.
17. Kopperdahl DL, Keaveny TM. Yield strain behavior of trabecular bone. *J Biomech* 1998;31:601–8.
18. Morgan EF, Keaveny TM. Dependence of yield strain of human trabecular bone on anatomic site. *J Biomech* 2001;34:569–77.
19. Dougherty G, Newman D. Measurement of thickness and density of thin structures by computed tomography: a simulation study. *Med Phys* 1999;26:1341–8.
20. Prevrhal S, Engelke K, Kalender WA. Accuracy limits for the determination of cortical width and density: the influence of object size and CT imaging parameters. *Phys Med Biol* 1999;44:751–64.
21. Faulkner KG, Cann CE, Hasegawa BH. Effect of bone distribution on vertebral strength: assessment with patient-specific nonlinear finite element analysis. *Radiology* 1991;179:669–74.
22. Rockoff SD, Sweet E, Bleustein J. The relative contribution of trabecular and cortical bone to the strength of human lumbar vertebrae. *Calcif Tissue Res* 1969;3:163–75.
23. Ito M. Assessment of bone quality using micro-computed tomography (micro-CT) and synchrotron micro-CT. *J Bone Miner Metab* 2005;23(suppl):115–21.
24. Silva MJ, Keaveny TM, Hayes WC. Computed tomography-based finite element analysis predicts failure loads and fracture patterns for vertebral sections. *J Orthop Res* 1998;16:300–8.
25. Martin H, Werner J, Andresen R, et al. Noninvasive assessment of stiffness and failure load of human vertebrae from CT-data. *Biomed Tech* 1998;43:82–8.
26. Liebschner MA, Kopperdahl DL, Rosenberg WS, et al. Finite element modeling of the human thoracolumbar spine. *Spine* 2003;28:559–65.
27. Crawford RP, Cann CE, Keaveny TM. Finite element models predict in vitro vertebral body compressive strength better than quantitative computed tomography. *Bone* 2003;33:744–50.
28. Crawford RP, Rosenberg WS, Keaveny TM. Quantitative computed tomography-based finite element models on the human lumbar vertebral body: effect of element size on stiffness, damage, and fracture strength predictions. *J Biomech Eng* 2003;125:434–8.
29. Eckstein F, Lochmüller EM, Lill CA, et al. Bone strength at clinically relevant sites displays substantial heterogeneity and is best predicted from site-specific bone densitometry. *J Bone Miner Res* 2002;17:162–71.

Copyright © Lippincott Williams & Wilkins. Unauthorized reproduction of this article is prohibited.

Osteoporos Int
DOI 10.1007/s00198-008-0750-8

ORIGINAL ARTICLE

Assessment of vertebral fracture risk and therapeutic effects of alendronate in postmenopausal women using a quantitative computed tomography-based nonlinear finite element method

K. Imai · I. Ohnishi · T. Matsumoto · S. Yamamoto · K. Nakamura

Received: 31 October 2007 / Accepted: 21 July 2008
© International Osteoporosis Foundation and National Osteoporosis Foundation 2008

Abstract
Summary A QCT-based nonlinear FEM was used to assess vertebral strength and mechanical parameters in postmenopausal women. It had higher discriminatory power for vertebral fracture than aBMD and vBMD. Alendronate effects were detected at 3 months, and marked bone density increases were noted in juxta-cortical areas compared to inner trabecular areas.
Introduction QCT-based finite element method (QCT/FEM) can predict vertebral compressive strength ex vivo. This study aimed to assess vertebral fracture risk and alendronate effects on osteoporosis in vivo using QCT/FEM.
Methods Vertebral strength in 104 postmenopausal women was analyzed, and the discriminatory power for vertebral fracture was assessed cross-sectionally. Alendronate effects were also prospectively assessed in 33 patients with postmenopausal osteoporosis who were treated with alendronate for 1 year.
Results On the age and body weight adjusted logistic regression, vertebral strength had stronger discriminatory power for vertebral fracture (OR per SD change: 6.71) than areal BMD and volumetric BMD. The optimal point for the vertebral fracture threshold was 1.95 kN with 75.9% sensitivity and 78.7% specificity. At 3 months, vertebral strength significantly increased by 10.2% from baseline. The minimum principal strain distribution showed that the area of high fracture risk decreased. At 1 year, the density of the inner cancellous bone increased by 8.3%, while the density of the juxta-cortical area increased by 13.6%.
Conclusions QCT/FEM had higher discriminatory power for vertebral fracture than BMD and detected alendronate effects at 3 months. Alendronate altered density distributions, thereby decreasing the area with a high fracture risk, resulting in increased vertebral strength.

Keywords Alendronate · Bone mechanics · Finite element method · Fracture risk · Osteoporosis · Vertebral strength

K. Imai · I. Ohnishi (✉) · T. Matsumoto · K. Nakamura
Department of Orthopaedic Surgery, School of Medicine,
The University of Tokyo,
7-3-1 Hongo, Bunkyo-ku,
Tokyo 113-0033, Japan
e-mail: ohnishii-dis@h.u-tokyo.ac.jp

K. Imai · S. Yamamoto
Department of Orthopaedic Surgery,
Tokyo Metropolitan Geriatric Medical Center,
35-2 Sakae-cho, Itabashi-ku,
Tokyo 173-0034, Japan

Introduction

Osteoporosis is defined as a skeletal disorder characterized by decreased bone strength and increased risk of fracture. Bone strength primarily reflects bone density and bone quality, which are influenced by bone architecture, turnover, accumulation of damage, and mineralization [1]. Measurements of areal bone mineral density (aBMD) using dual energy X-ray absorptiometry (DXA) and bone turnover markers have been the standard methods for diagnosing osteoporosis, in addition to assessing fracture risk and therapeutic effects. However, spinal aBMD only explains 50–80% of vertebral strength [2–6], and the application of aBMD measurements in isolation cannot identify individuals who eventually experience bone fracture because of the low sensitivity of the test [7]. Levels of bone turnover markers may identify changes in bone remodeling within a relatively short interval before aBMD changes can be detected, but do not predict

bone strength or fracture risk and are only weakly associated with changes in bone strength [1].

The finite element method (FEM), an engineering computational method of mechanical analysis for complex structures, has been used to study the mechanics of human bone. A FEM based on data from quantitative computed tomography (QCT) has been applied to predict proximal femoral fracture [8–12]. QCT-based FEM appears more predictive of femoral strength than QCT or DXA alone [8] and can predict proximal femoral fracture location [10]. Nonlinear FEM demonstrated improved predictions of femoral strength [11]. For the spine, QCT-based nonlinear FEM was clinically applied to assess vertebral strength [13], and cadaver studies have been performed to evaluate the accuracy of QCT-based FEM [14–19]. The cadaver studies have verified that QCT-based FEM predicts failure loads and fracture patterns for 10-mm-thick vertebral sections [14] and can predict ex vivo vertebral compressive strength better than BMD [15, 16] and QCT alone [17].

QCT-based nonlinear FEM can accurately predict vertebral strength, fracture sites, and distribution of minimum principal strain ex vivo [19]. Based on verification by the cadaver studies, FEM has been applied clinically to the assessment of chronic glucocorticoid treatment at the hip [20], as well as teriparatide and alendronate sodium (alendronate) treatment for osteoporosis at the lumbar spine [21], proving useful for assessing medication effects on bone strength. A recent paper showed that FEM is a significant parameter of vertebral fracture risk [22]. However, little data is available about the optimal value of vertebral strength for the vertebral fracture threshold. In addition, little information is available about FEM assessment of medication effects in a short interval before aBMD changes can be detected.

The purpose of this study was to analyze vertebral strength in postmenopausal Japanese women using a QCT-based nonlinear FEM (QCT/FEM) in vivo and then to evaluate the discriminatory power for vertebral fracture. The relationship between analyzed vertebral strength index and the incidence of previous vertebral fractures was evaluated in a cross-sectional manner, and a cutoff point for vertebral fracture threshold was determined. We also prospectively assessed the effects of alendronate for patients with postmenopausal osteoporosis from analyzed vertebral strength index and mechanical parameters and then examined the mechanism of alendronate treatment from a biomechanical perspective.

Materials and methods

Study design and participants

This study was conducted at Tokyo Metropolitan Geriatric Medical Center in Tokyo, Japan. The study protocol was approved by the ethics committee, and each participant provided written informed consent in accordance with the Declaration of Helsinki.

The inclusion criteria included ambulatory postmenopausal Japanese women aged between 49 and 85 years old. Exclusion criteria included women with any disorders of bone and mineral metabolism other than postmenopausal osteoporosis, those who had any recent or current treatment with the potential to alter bone turnover or bone metabolism, and those with a history of second lumbar vertebral (L2) fracture. Osteoporosis was diagnosed based on the lumbar spine aBMD measured using DXA as <70% of the average aBMD of young healthy Japanese women or by the presence of radiographic vertebral fracture [23]. Vertebral fracture was diagnosed based on lateral spine radiography. Radiographic vertebral fracture was defined if either the anterior or central height was ≥20% less than posterior height.

A total of 123 eligible participants were enrolled in this cross-sectional study. Among these, 70 patients were diagnosed with osteoporosis, and 37 patients were enrolled in the prospective study assessing the therapeutic effects of alendronate. All 37 participants were treated using oral alendronate at a dose of 5 mg/day.

DXA, QCT, and QCT/FEM

For all participants, aBMD of the anteroposterior (AP) lumbar spine (L2–4) and total hip were measured by DXA (DPX; Lunar, Madison, WI, USA). Axial QCT scans of L2 were obtained with a slice thickness of 2 mm and a pixel width of 0.35 mm using Light Speed QX/i (GE Yokokawa Medical System, Tokyo, Japan; 120 kV, 360 mA, 512×512 matrix) with a calibration phantom containing hydroxyapatite rods. In these central sections, mid-vertebral trabecular volumetric BMD (vBMD) was measured. A cylindrical region of interest (ROI) with a radius of 10 mm and a thickness of 10 mm was placed manually in the vertebral body, excluding the cortical bone. Hounsfield unit values in the ROI were transformed into equivalent density.

A three-dimensional FEM was constructed from QCT data using Mechanical Finder software (Mitsubishi Space Software, Tokyo, Japan) [12, 19] with 2-mm tetrahedral elements and 2-mm triangular plates. The Young's modulus and the thickness of each triangular plate were assigned values of 10 GPa and 0.4 mm, respectively. However, these plate elements model only the outer surface of the cortical shell. If the cortical shell was thicker than the plate element, the whole cortical area was modeled, incorporating the tetrahedral elements adjacent to the triangular plates, as well as the plate elements.

To allow for bone heterogeneity, mechanical properties of each element were computed from the Hounsfield unit value. Ash density was derived from the phantom BMD,

which is almost equivalent to that of the hydroxyapatite as shown in our previous paper [12]. Ash density of each voxel was determined using the linear regression equation created from values of the calibration phantom. Ash density of each element was set as the average ash density of the voxels contained in one element. Young's modulus and yield stress of each tetrahedron element were calculated from the equations proposed by Keyak et al. [9]. Poisson's ratio of each element was set as 0.4.

Boundary conditions were applied with all the elements and all the nodes of the lower end of the vertebral model completely restrained. A uniaxial compressive load with a uniform distribution and a uniform load increment was applied, and the fracture load was analyzed using Mechanical Finder as previously reported [19]. Each element was assumed to yield when its Drucker–Prager equivalent stress reached the element yield stress. Failure was defined as occurring when the minimum principal strain of the first element was less than −10,000 microstrain. Vertebral yield was defined as occurring when at least one element yielded while vertebral fracture was defined as being when at least one element failed. Fracture load was defined as the vertebral strength index. Characteristics of our model included adoption of the tetrahedral elements to model surface curvature of the entire vertebra, utilization of materially nonlinear analysis to match elastoplasticity of the vertebra during compression, construction of a cortical shell as the surface of the model, and the adoption of Drucker–Prager equivalent stress instead of von-Mises stress as a criterion of element yield. Accuracy of the calculated vertebral strength, fracture site, and minimum principal strain at the vertebral surface throughout the loading process has been verified in a cadaver study [19]. On repeating the FE analysis five times for each of the 12 QCT data in our previous cadaver study, the coefficient of variation (CV) for the measurement of vertebral compressive strength was 0.96%. The accuracy of QCT/FEM with an element size of 2 mm has been verified in a convergence study [24].

Assessment of alendronate effects

In patients who were enrolled in the study for assessing the therapeutic effects of alendronate, axial QCT scans of L2 were obtained at baseline and 3, 6, and 12 months. The vBMD was measured and vertebral strength was analyzed using the QCT/FEM. The aBMD of the AP lumbar spine (L2–4) and the total hip were measured by DXA at baseline and 6 and 12 months. Measurement of urinary N-telopeptide of type-collagen (NTx) as a biochemical marker of bone resorption was performed at baseline and 3 months. In the follow-up period, four subjects were excluded due to the occurrence of adverse events (n=2) or L2 fracture (n=2). The 33 remaining patients [mean (±SD) age, 76.5±5.4 years] were included in the prospective study for assessment of the therapeutic effects of alendronate. The control group comprised eight postmenopausal women without any drug therapy for osteoporosis (mean age, 76.3±6.4 years).

To assess the effects of alendronate therapy on biomechanical behaviors, distribution of minimum principal strain within vertebrae was analyzed using the QCT/FEM with an applied load of 1 kN, under which all specimens were in the elastic phase. Density distribution was also analyzed by QCT/FEM. Density of the cancellous bone, removing the outer 2 mm of each vertebra, and density of the cortical and juxta-cortical bone of the outer 2 mm were calculated separately.

Statistical analysis

For statistical analysis, the Kruskal–Wallis test and Mann–Whitney test were used to compare L2–4 aBMD measured by DXA, total hip aBMD measured by DXA, L2 vBMD measured by QCT, and L2 vertebral strength index analyzed by QCT/FEM among the different subject groups. Logistic regression analysis was performed to estimate risk factors for vertebral fracture. L2–4 aBMD, total hip aBMD, vBMD, and vertebral strength index were assessed using sensitivity and specificity curves to determine the optimal cutoff point as the vertebral fracture threshold.

Paired t tests were used to evaluate alendronate effect by comparisons between baseline and each time-point regarding L2–4 aBMD, total hip aBMD, vBMD, vertebral strength index, and urinary NTx. Friedman tests were used to evaluate mean percent changes from baseline in L2–4 aBMD and vertebral strength index. For each statistical analysis, differences were considered significant at $p<0.05$. Statistical analysis was performed using StatView for Windows version 5.0 software (SAS Institute, Cary, NC, USA).

Results

Assessment of vertebral fracture risk

The 123 women enrolled in the study had a mean age of 71.8±7.4 years, mean height of 149.4±5.6 cm, and mean weight of 50.2±7.4 kg. L2–4 aBMD was 0.816±0.191 g/cm^2, total hip aBMD was 0.693±0.103 g/cm^2, L2 vBMD was 72.8±26.0 mg/cm^3, and L2 vertebral strength index was 2.26±0.80 kN.

Subjects were classified into 5-year age groups, summarized in Table 1. Among the 5-year age groups, significant decreases were identified in vBMD (Kruskal–Wallis test, p=0.001) and analyzed vertebral strength index (p=0.001) in the older age groups. However, L2–4 aBMD (p=0.410)

Table 1 Summary of the subjects' height, weight, L2–4 aBMD, total hip aBMD, L2 vBMD, and L2 vertebral strength index

Age (years)	49–59 (n=8)	60–64 (n=12)	65–69 (n=20)	70–74 (n=31)	75–79 (n=37)	80–85 (n=15)
Height (cm)	155.0±3.5	150.8±5.1	152.3±6.2	148.7±4.7	148.4±5.6	145.1±3.8
Weight (kg)	49.4±2.8	49.9±6.9	50.7±6.4	51.7±8.7	48.9±8.0	50.3±6.3
L2–4 aBMD (g/cm^2)	0.874±0.135	0.850±0.180	0.835±0.115	0.744±0.169	0.824±0.232	0.867±0.191
Total hip aBMD (g/cm^2)	0.708±0.071	0.762±0.083	0.738±0.080	0.701±0.107	0.653±0.105	0.688±0.103
L2 vBMD (mg/cm^3)	111.4±22.2	88.6±23.5	74.7±16.3	72.7±25.2	66.5±24.6	52.4±18.9
Vertebral strength index (kN)	3.41±1.11	2.31±0.67	2.64±0.68	2.10±0.75	2.05±0.70	1.93±0.51

Values are mean±SD.
QCT L2 vBMD and vertebral strength index decreased significantly in the older age groups, $p<0.05$ (Kruskal–Wallis test).

and total hip aBMD (p=0.112) did not show any significant differences.

Next, subjects were classified on the basis of prior vertebral fracture. Among the 123 women, 75 subjects did not have any vertebral fractures (nonfracture group), and 48 subjects already had vertebral fractures (fracture group). Vertebral fractures were present in 39.0% of the total study population. Among the fracture group, vertebral fractures spontaneously developed in 29 women (spontaneous fracture group) and were caused by trauma in 19 women (traumatic fracture group). Among the 19 subjects in the traumatic fracture group, 18 women developed fracture following a fall from standing height, and one woman developed fracture following a fall down stairs.

Group characteristics are summarized in Table 2. To exclude factors of trauma, 75 subjects in the nonfracture group and 29 subjects in the spontaneous fracture group were compared. L2–4 aBMD (Mann–Whitney test, p= 0.0033) and total hip aBMD (p=0.0105) were significantly decreased in the spontaneous fracture group compared with the nonfracture group. L2 vBMD and vertebral strength index showed greater significance ($p<0.0001$). Logistic regression analysis after adjustment for age and body weight revealed vBMD reduction and vertebral strength index reduction as risk factors associated with spontaneous vertebral fracture (Table 3).

L2–4 aBMD, total hip aBMD, vBMD, and vertebral strength index were assessed by sensitivity and specificity curves. The nonfracture group and spontaneous fracture group (104 women in total) were assessed in a cross-sectional manner. The optimal point on the sensitivity and specificity curves used as the fracture threshold to predict spontaneous vertebral fractures for L2 vertebral strength index was 1.95 kN with 75.9% sensitivity and 78.7% specificity (Fig. 1). The optimal point for L2–4 aBMD was 0.816 g/cm^2 (−2.62 SD compared to young healthy Japanese women) with 69.0% sensitivity and 72.0% specificity, and the optimal point for total hip aBMD was 0.664 g/cm^2 with 55.1% sensitivity and 58.7% specificity. The optimal point for L2 vBMD was 60.8 mg/cm^3 with 75.9% sensitivity and 76.0% specificity. The area under the receiver operator characteristic (ROC) curve for the vertebral strength index was 0.822, which was significantly larger than that for L2–4 aBMD (area=0.713, p=0.0010), hip aBMD (area=0.682, $p<0.0001$), and L2 vBMD (area= 0.767, p=0.0129; Fig. 2).

Assessment of alendronate effects

Subjects comprised 33 women with postmenopausal osteoporosis receiving alendronate therapy for 12 months and eight postmenopausal women without any drug therapy for osteoporosis as controls.

In the alendronate treatment group, significant increases from baseline in L2–4 aBMD (paired t-test, $p<0.0001$) and vBMD (p=0.0013) were seen at 12 months (Table 4).

Table 2 Characteristics of participants in nonfracture, spontaneous fracture, and traumatic fracture groups

	Nonfracture (n=75)	Spontaneous fracture (n=29)	Traumatic fracture (n=19)
Age (years)	69.5±7.7	76.0±4.8	74.7±5.6
Height (cm)	150.6±5.1	147.5±5.4	147.4±6.6
Weight (kg)	51.5±7.3	47.8±6.9	48.7±7.6
L2–4 aBMD (g/cm^2)	0.860±0.166	0.719±0.209*	0.831±0.190
Total hip aBMD (g/cm^2)	0.710±0.092	0.634±0.102*	0.723±0.111
L2 vBMD (mg/cm^3)	80.3±24.2	51.5±22.0**	75.7±21.8
Vertebral strength index (kN)	2.55±0.78	1.59±0.51**	2.12±0.56

Values are mean±SD.
*$p<0.05$ and **$p<0.0001$ (Mann–Whitney test), between spontaneous fracture group and nonfracture group.

Table 3 Risk factors associated with spontaneous vertebral fracture adjusted for age and body weight

Variable	Odds ratio	95% CI	*p* Value
L2–4 aBMD (per SD)	1.83	1.13–3.26	0.0238
Total hip aBMD (per SD)	1.73	0.69–4.71	0.2554
L2 vBMD (per SD)	3.57	1.73–8.64	0.0017
Vertebral strength index (per SD)	6.71	2.85–19.46	<0.0001

Significant increases in vertebral strength index from baseline were noted at 3, 6, and 12 months ($p<0.0001$). A significant decrease from baseline was seen in urinary NTx at 3 months ($p<0.0001$). All 33 subjects showed decreased urinary NTx at 3 months from baseline. Regarding vertebral strength index, 29 patients showed increases at 3 months, 32 patients showed increases at 6 months, and all patients showed increases at 12 months. Regarding L2–4 aBMD, 24 patients showed increases at 6 months, and 28 patients showed increases at 12 months. The mean percentage increase in vertebral strength index from baseline to 3 months was 10.2%. At 6 months, mean percentage increase from baseline was 16.7% in vertebral strength index and 3.7% in L2–4 aBMD. At 12 months, mean percentage increase from baseline was 26.9% in vertebral strength index and 7.5% in L2–4 aBMD (Fig. 3). Percentage increases in the vertebral strength index were significant at baseline, 3, 6, and 12 months (Friedman test, $p<0.0001$), and the percentage increases in L2–4 aBMD were significant at baseline, 6, or 12 months ($p=0.0278$), although the percentage increases in vBMD were not significant at baseline, 3, 6, or 12 months ($p=0.0731$).

In the untreated control group, the average L2–4 aBMD was 0.822±0.136 g/cm^2 at baseline and 0.817±0.166 g/cm^2 at 12 months. The average total hip aBMD was 0.701±0.085 g/cm^2 at baseline and 0.696±0.091 g/cm^2 at 12 months. The average L2 vBMD was 61.1±16.8 mg/cm^3 at baseline and 60.9±13.5 mg/cm^3 at 12 months. The average L2 vertebral strength index was 2.26±0.70 kN at baseline and 2.24±0.67 kN at 12 months. The average urinary NTx was 58.8±18.2 nmol BCE/mmol Cr at baseline and 59.3±14.6 nmol BCE/mmol at 3 months. None of the values showed significant changes (Table 4).

In the alendronate treatment group, comparison of change from baseline to 3 months for each subject indicated a low correlation between percentage change in vertebral strength index and percentage change in urinary NTx ($r=0.295$, $p=0.0955$). The correlation between percentage change in vertebral strength index and percentage change in L2–4 aBMD at 12 months was moderate ($r=0.481$, $p=0.0046$).

The distribution of minimum principal strain analyzed by QCT/FEM at the midsagittal section with an applied load of 1 kN showed that the area with less than −10,000 microstrain of minimum principal strain at baseline, where a high risk of fracture exists [19], had decreased during alendronate therapy (Fig. 4). In five of the 33 patients, L2–4 aBMD decreased, although vertebral strength index in all 33 patients increased from baseline at 12 months. In one patient with a discrepancy between changes in L2–4 aBMD (3.7% decrease) and vertebral strength index (23.3% increase), density distribution showed increased density in the juxta-cortical bone and distribution of minimum principal strain showed improved strain in the area with less than −10,000 microstrain of minimum principal strain during alendronate therapy (Fig. 5). Mean percentage increase from baseline to 12 months in density of inner cancellous bone with a distance of >2 mm from the outer surface was 8.3% (paired *t* test, $p=0.0013$), while the density of cortical and juxta-cortical bone with a thickness of 2 mm increased by 13.6% ($p=0.0004$).

Discussion

In the treatment of osteoporosis, the target is to assess fracture risk, and the end-point is to prevent fractures. The World Health Organization (WHO) set the criterion for

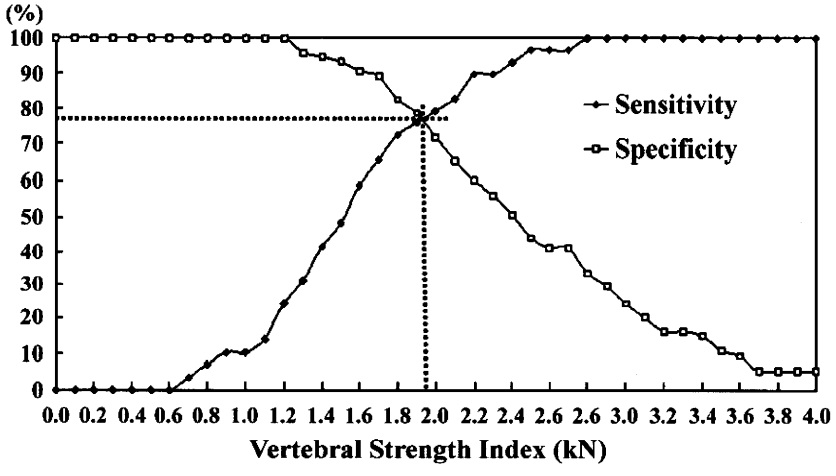

Fig. 1 Sensitivity and specificity curves to determine the optimal cutoff point of the vertebral strength index analyzed by QCT/FEM for the vertebral fracture threshold. The optimal point for vertebral strength was 1.95 kN with 75.9% sensitivity and 78.7% specificity

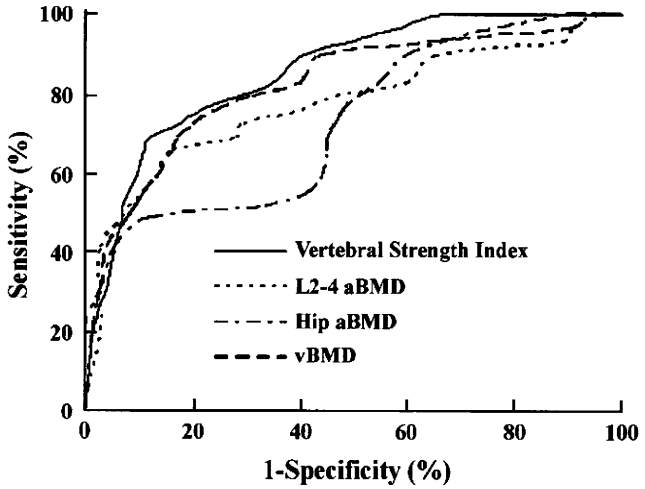

Fig. 2 ROC curves showing 1-specificity (false-positive rate) vs. sensitivity (true positive rate) for the vertebral strength index, L2–4 aBMD, hip aBMD, and vBMD

diagnosing osteoporosis in Caucasian women as aBMD at ≥2.5 SDs below the normal aBMD for young healthy Caucasian women, based on data that this criterion identified 30% of all postmenopausal women as having osteoporosis, more than half of whom would have sustained a prior fracture [25]. However, meta-analysis of prospective cohort studies concluded that measurements of aBMD could not identify individuals who would have future fractures due to a low sensitivity of <50% and high false-positive rate of 15% [7].

The present results show that QCT/FEM had higher sensitivity and specificity for spontaneous vertebral fracture discrimination than L2–4 aBMD, total hip aBMD, and L2 vBMD. A recent paper on the cross-sectional assessment of vertebral fracture risk using a CT-based FEM reported that the odds ratio (OR) per SD decrease was 2.2 with 1.1–4.3 of 95% confidence interval (CI), and the area under the ROC curve was 0.80 for vertebral compressive strength, while the OR per SD decrease was 0.7 (95% CI, 0.4–1.2) and the area under the ROC curve was 0.75 for spinal aBMD measured using DXA [22]. The results of our study showed a higher OR (6.71; 95% CI, 2.85–19.46) and a greater area under the ROC curve (0.822) for vertebral compressive strength than for spinal aBMD (OR, 1.83; 95% CI, 1.13–3.26; area, 0.713). However, it would be difficult to directly compare the results of our study with those of another study because they were different cohorts in terms of size, age, and geographic location.

The cutoff value of vertebral strength index for predicting vertebral fractures without trauma was 1.95 kN, equivalent to 3.94 times the mean subject body weight of 50.5 kg. Low trauma fractures such as a fall from a standing height are due to osteoporosis. The present assessment excluded the traumatic fracture group. Therefore, the threshold value was not for diagnosing osteoporosis, but for assessing spontaneous vertebral fracture risk.

Alendronate is a bisphosphonate that potently inhibits bone resorption and is widely used for the treatment of osteoporosis. Alendronate produces a sustained reduction in levels of biochemical markers of bone remodeling, returning these to the premenopausal range, and also increases aBMD and decreases the risk of osteoporotic fracture in postmenopausal women [26–32]. The results in this study show that QCT/FEM can detect the therapeutic effects of alendronate at 3 months. All 33 patients who received alendronate therapy showed increased vertebral strength index at 12 months from baseline, indicating that all patients gained therapeutic effects. At 3 months, four patients did not show therapeutic effects on vertebral strength index, although all patients showed decreased urinary NTx. On L2–4 aBMD, five patients did not show therapeutic effects at 12 months. These results indicate that therapeutic effects of alendronate can be detected first in the biochemical markers of bone resorption, then in vertebral strength index, and then finally in L2–4 aBMD. A low correlation existed between percentage change in vertebral strength index and that in urinary NTx. Vertebral strength index analyzed by QCT/FEM thus does not incorporate effects on bone turnover. The correlation between percentage change in vertebral strength index and that in L2–4 aBMD was moderate. As QCT/FEM was a better predictor

Table 4 Mean percentage changes from baseline values at 6 and 12 months

	Alendronate 5 mg/day (n=33)		Untreated control group (n=8)	
	6 months	12 months	6 months	12 months
L2–4 aBMD	3.7	7.5**	−0.3	−0.9
Total hip aBMD	0.2	0.9	−0.1	−0.7
L2 vBMD	5.1	8.8*	−0.2	−0.7
Vertebral Strength index	16.7**	26.9**	−0.3	−0.8
Inner cancellous bone density	5.2	8.3*	−0.3	−0.7
Juxta-cortical bone density	8.0*	13.6*	−0.3	−0.8

*p<0.05 and **p<0.0001 (paired t test), compared with baseline.

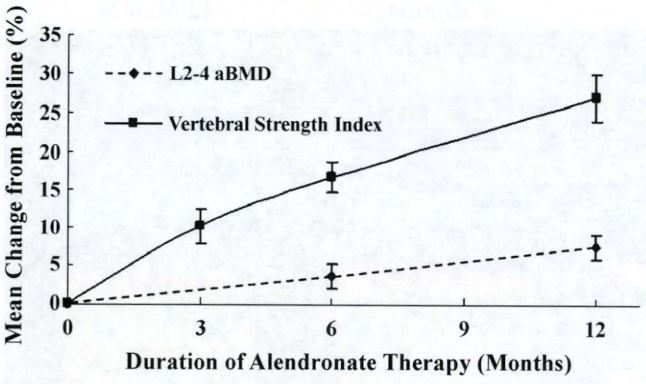

Fig. 3 Mean (±SE of mean) changes from baseline values in L2–4 aBMD measured by DXA and L2 vertebral strength index analyzed by QCT/FEM in women with postmenopausal osteoporosis receiving alendronate therapy for 12 months

than L2–4 aBMD, vertebral strength index might incorporate the effects on other factors as well as aBMD.

Another recent study investigating the effects of teriparatide and alendronate on vertebral strength using a CT-based FEM reported that the mean percentage increase in vertebral compressive strength with alendronate therapy was 4.9% at 6 months and 3.7% at 18 months, which suggests that vertebral strength reached a plateau after 6 months of alendronate therapy [21]. There is a discrepancy between the above results and our results, in which vertebral strength continued to increase from 6 to 12 months of alendronate therapy. In addition, our result showed that after alendronate therapy, there was a moderate correlation between the percentage change in vertebral strength on FEM and that on spinal aBMD using DXA (p=0.0046), although Keaveny et al. reported there was no significant correlation between these two (p=0.895) [21]. Our FEM differs from that of Keaveny in many aspects. But both of these analysis techniques have been shown to provide estimates of vertebral compressive strength that correspond closely with direct ex vivo biomechanical measurements for cadaveric vertebrae. Therefore, the differences in the finite element analysis technique might not greatly affect the results. In our results, the increase of the strength was larger and persistent throughout a year. Conversely, the increase of strength in Keaveny's study plateaued from 6 to 18 months. This might be due to the difference in patient background. The patients treated with alendronate in our study were older, with a mean age of 76.5 years, compared to 62.5 years in Keaveny's study. Then, in our study, the average baseline spine trabecular vBMD was 56.2 mg/cm^3, but it was 85.7 mg/cm^3 in Keaveny's study. The lower spine vBMD at baseline could contribute to the larger increase of the vBMD and the predicted strength in our study.

The QCT/FEM result revealed that density of the cortical and juxta-cortical bone with a thickness of 2 mm from the outer surface increased more than that of the inner cancellous bone with a distance of >2 mm, indicating that alendronate treatment was more effective in cortical and juxta-cortical areas compared to the inner trabecular compartment. Changes in cortical and juxta-cortical areas were not incorporated into changes in vBMD, which reflected only the inner trabecular compartment. The correlation between vertebral strength index and vBMD was r=0.757 (p<0.0001). In this study, the precision of vBMD was relatively poor with manual placement of the ROI, the inclusion of only a single vertebral level and the exclusion of the outer trabecular bone. In contrast, our QCT/FEM included cortical areas by construction of a cortical shell to the model. As a result, vBMD might fail to accurately assess spontaneous vertebral fracture risk and detect the therapeutic effects of alendronate. With a more optimized vBMD analysis, its accuracy for assessing vertebral fracture risk and detecting alendronate effects might have more closely matched that of QCT/FEM.

An in vivo study to assess the effects of teriparatide and alendronate therapy for osteoporosis reported that after 18 months of alendronate treatment, trabecular vBMD measured by QCT in the femoral neck increased by 2.2% from baseline and cortical vBMD increased significantly by 7.7%, supporting our result [33]. In the teriparatide group, trabecular vBMD increased significantly by 4.9%, but cortical vBMD decreased by 1.2% [33]. In contrast, another in vivo study reported that after 12 months of alendronate treatment, the trabecular vBMD measured by QCT at the spine (L1 and L2) increased by 10.5% from baseline, but the integral density (cortical and trabecular bone) at the spine changed much less [34]. With the currently available

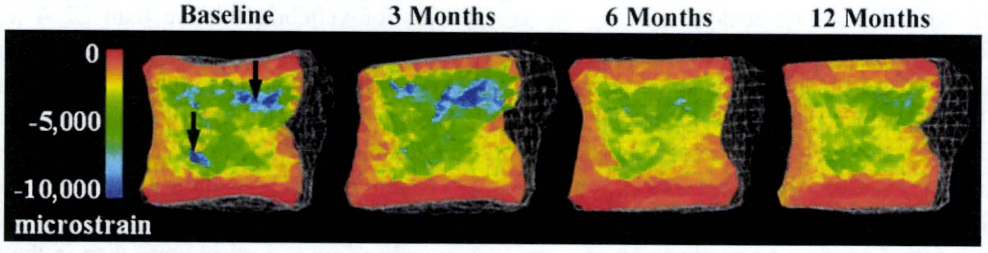

Fig. 4 Distribution of minimum principal strain at the midsagittal section with an applied load of 1 kN as analyzed by QCT/FEM. The area displaying less than −10,000 microstrain of minimum principal strain at baseline (*arrows*), with high risk of fracture, is decreased after 6 and 12 months of alendronate therapy

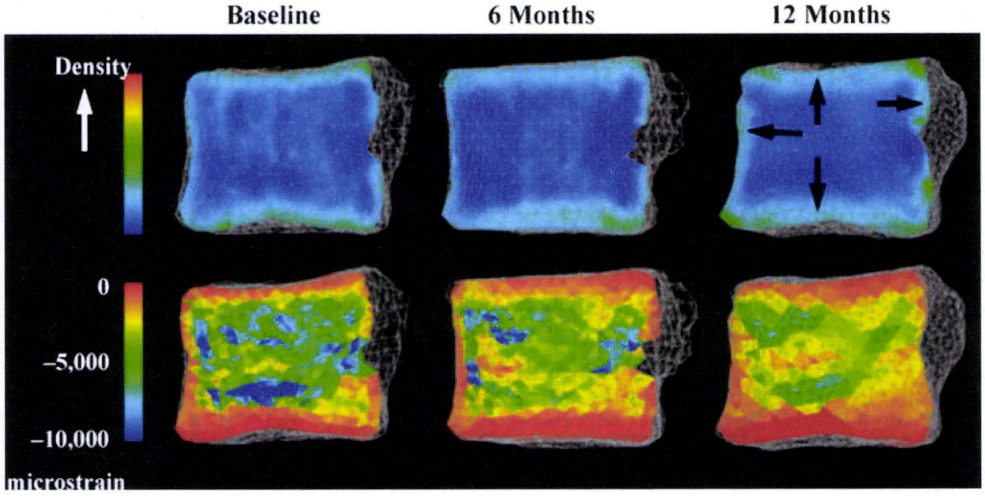

Fig. 5 Distribution of density and minimum principal strain. The density distribution shows an increased density in the juxta-cortical region (*arrows*). The area with a large negative value (for example, less than −10,000 microstrain) of the minimum principal strain narrowed after 12 months of alendronate therapy compared with the same area at baseline

CT resolution, at a pixel spacing larger than 0.25 mm, the thin cortical shell of vertebral bone cannot be precisely evaluated, and its density tends to be underestimated [35, 36]. Therefore, we constructed a cortical shell, which would contribute to the assessment of the cortical density. However, it may be necessary to investigate this further using QCT with improved resolution.

Secondary mineralization in cortical and cancellous bone was reportedly prolonged after alendronate therapy in osteoporotic women [37]. Porosity in cortical bone was also markedly decreased after alendronate therapy in osteoporotic women [38]. Increased bone density in cortical and juxta-cortical areas might be attributable to prolonged secondary mineralization and decreased cortical porosity.

In the patient with decreased L2–4 aBMD, density in the juxta-cortical area was increased, and the area where a high risk of fracture existed had decreased during alendronate therapy. Alendronate might alter the distribution of density, thereby improving the distribution of minimum principal strain, increasing vertebral strength. Alterations in the distribution of density would therefore represent one of the factors incorporated by QCT/FEM. A meta-analysis study reported that improvements in spinal aBMD explain only 16% of the reduction in the risk of vertebral fracture with alendronate [39]. QCT/FEM might supply a portion of deficit that aBMD cannot explain regarding vertebral fracture reduction with alendronate therapy.

Bone remodeling is regulated by signals due to both mechanical strain and microdamage when damage is below a certain threshold, but causes osteocyte apoptosis when damage is above a critical level, so that a remodeling response occurs to remove the dead osteocytes [40]. Whether alendronate effects are regulated by various mechanical parameters is unknown. Investigating mechano-sensors and mechano-receptors that regulate therapeutic effects is a target for future study.

Some limitations are apparent regarding the analysis in this study. First, QCT/FEM cannot detect microdamage and bone turnover. In clinical application, other parameters such as age and bone turnover markers should be included to assess the risk of fracture and therapeutic effects. Second, analysis was performed under a simple compressive loading condition. Analysis under a fall loading condition will be one of the assignments in a future study. Third, the risk of fracture was assessed cross-sectionally, although the ultimate goal is to assess the risk of fracture prospectively. Large-scale, prospective cohort studies over a long time period are needed to assess the threshold for discriminating the risk of vertebral fracture. Fourth, we used the same criteria throughout the alendronate therapy, assuming that none of the mechanical properties were altered. This assumption is based on a study which found that, in ovariectomized baboons, 2 years of alendronate treatment did not alter the mechanical properties of cortical tissue or the nonlinear strength-density correlation for trabecular bone [41]. In addition, a study on healthy male dogs showed that 23 weeks of alendronate treatment did not alter mechanical properties of trabecular bone [42]. Other limitations were that this study was a nonrandomized drug study, and only eight subjects were included in the untreated group. A randomized controlled clinical trial is required to confirm our results.

In conclusion, QCT/FEM had higher discriminatory power for vertebral fracture than L2–4 aBMD, total hip aBMD, and L2 vBMD. The cutoff value of vertebral strength index for predicting vertebral fractures without trauma was 1.95 kN, equivalent to 3.94 times body weight. In addition, QCT/FEM could detect the therapeutic effects of alendronate at 3 months. The distribution of density revealed that alendronate treatment was more effective in cortical and juxta-cortical areas than in the inner trabecular compartment. Alendronate might alter distributions of density, thereby improving the distribution of minimum

principal strain and resulting in increased vertebral strength. QCT/FEM is useful for assessing the risk of vertebral fracture and therapeutic effects on osteoporosis and provides unique theories from a biomechanical perspective.

Acknowledgments This work was funded by a grant in aid for Scientific Research received from the Japan Society for the Promotion of Science (14657356).

Conflicts of interest None.

References

1. NIH Consensus Development Panel on Osteoporosis Prevention D, and Therapy (2001) Osteoporosis prevention, diagnosis, and therapy. JAMA 285:785–795
2. Edmondston SJ, Singer KP, Day RE et al (1994) In-vitro relationships between vertebral body density, size and compressive strength in the elderly thoracolumbar spine. Clin Biomech 9:180–186
3. Cheng XG, Nicholson PH, Boonen S et al (1997) Prediction of vertebral strength in vitro by spinal bone densitometry and calcaneal ultrasound. J Bone Miner Res 12:1721–1728
4. Eriksson SA, Isberg BO, Lindgren JU (1989) Prediction of vertebral strength by dual photon absorptiometry and quantitative computed tomography. Calcif Tissue Int 44:243–250
5. Myers BS, Arbogast KB, Lobaugh B et al (1994) Improved assessment of lumbar vertebral body strength using supine lateral dual-energy X-ray absorptiometry. J Bone Miner Res 9:687–693
6. Bjarnason K, Hassager C, Svendsen OL et al (1996) Anteroposterior and lateral spinal DXA for the assessment of vertebral body strength: comparison with hip and forearm measurement. Osteoporos Int 6:37–42
7. Marshall D, Johnell O, Wedel H (1996) Meta-analysis of how well measures of bone mineral density predict occurrence of osteoporotic fractures. BMJ 312:1254–1259
8. Cody DD, Gross GJ, Hou FJ et al (1999) Femoral strength is better predicted by finite element models than QCT and DXA. J Biomech 32:1013–1020
9. Keyak JH, Rossi SA, Jones KA et al (1998) Prediction of femoral fracture load using automated finite element modeling. J Biomech 31:125–133
10. Keyak JH, Rossi SA, Jones KA et al (2001) Prediction of fracture location in the proximal femur using finite element models. Med Eng Phys 23:657–664
11. Keyak JH (2001) Improved prediction of proximal femoral fracture load using nonlinear finite element models. Med Eng Phys 23:165–173
12. Bessho M, Ohnishi I, Matsuyama J et al (2007) Prediction of strength and strain of the proximal femur by a CT-based finite element method. J Biomech 40:1745–1753
13. Faulkner KG, Cann CE, Hasegawa BH (1991) Effect of bone distribution on vertebral strength: assessment with patient-specific nonlinear finite element analysis. Radiology 179:669–674
14. Silva MJ, Keaveny TM, Hayes WC (1998) Computed tomography-based finite element analysis predicts failure loads and fracture patterns for vertebral sections. J Orthop Res 16:300–308
15. Martin H, Werner J, Andresen R et al (1998) Noninvasive assessment of stiffness and failure load of human vertebrae from CT-data. Biomed Tech 43:82–88
16. Buckley JM, Loo K, Motherway J (2007) Comparison of quantitative computed tomography-based measures in predicting vertebral strength. Bone 40:767–774
17. Crawford RP, Cann CE, Keaveny TM (2003) Finite element models predict in vitro vertebral body compressive strength better than quantitative computed tomography. Bone 33:744–750
18. Liebschner MA, Kopperdahl DL, Rosenberg D et al (2003) Finite element modeling of the human thoracolumbar spine. Spine 28:559–565
19. Imai K, Ohnishi I, Bessho M et al (2006) Nonlinear finite element model predicts vertebral bone strength and fracture site. Spine 31:1789–1794
20. Lian KC, Lang TF, Keyak JH et al (2005) Differences in hip quantitative computed tomography (QCT) measurements of bone mineral density and bone strength between glucocorticoid-treated and glucocorticoid-naive postmenopausal women. Osteoporos Int 16:642–650
21. Keaveny TM, Donley DW, Hoffmann PF et al (2007) Effects of teriparatide and alendronate on vertebral strength as assessed by finite element modeling of QCT scans in women with osteoporosis. J Bone Miner Res 22:149–157
22. Melton LJ III, Riggs BL, Keaveny TM et al (2007) Structural determinants of vertebral fracture risk. J Bone Miner Res 22:1885–1892
23. Orimo H, Hayashi Y, Fukunaga M et al (2001) Diagnostic criteria for primary osteoporosis: year 2000 revision. J Bone Miner Metab 19:331–337
24. Imai K, Ohnishi I, Yamamoto S et al (2008) In vivo assessment of lumbar vertebral strength in elderly women using computed tomography-based nonlinear finite element model. Spine 33:27–32
25. World Health Organization (1994) Assessment of fracture risk and its application to screening for postmenopausal osteoporosis. Report of a WHO Study Group. World Health Organ Tech Rep Ser 843:1–129
26. Devogelaer JP, Broll H, Correa-Rotter R et al (1996) Oral alendronate induces progressive increases in bone mass of the spine, hip, and total body over 3 years in postmenopausal women with osteoporosis. Bone 18:141–150
27. Tucci JR, Tonino RP, Emkey RD et al (1996) Effect of three years of oral alendronate treatment in postmenopausal women with osteoporosis. Am J Med 101:488–501
28. Black DM, Cummings SR, Karpf DB et al (1996) Randomised trial of effect of alendronate on risk of fracture in women with existing vertebral fractures. Fracture Intervention Trial Research Group. Lancet 348:1535–1541
29. Liberman UA, Weiss SR, Broll J et al (1995) Effect of oral alendronate on bone mineral density and the incidence of fractures in postmenopausal osteoporosis. The Alendronate Phase III Osteoporosis Treatment Study Group. N Engl J Med 333:1437–1443
30. Cummings SR, Black DM, Thompson DE et al (1998) Effect of alendronate on risk of fracture in women with low bone density but without vertebral fractures: results from the Fracture Intervention Trial. JAMA 280:2077–2082
31. Pols HA, Felsenberg D, Hanley DA et al (1999) Multinational, placebo-controlled, randomized trial of the effects of alendronate on bone density and fracture risk in postmenopausal women with low bone mass: results of the FOSIT study. Fosamax International Trial Study Group. Osteoporos Int 9:461–468
32. Ensrud KE, Black DM, Palermo L et al (1997) Treatment with alendronate prevents fractures in women at highest risk: results from the Fracture Intervention Trial. Arch Intern Med 157:2617–2624
33. McClung MR, San Martin J, Miller PD et al (2005) Opposite bone remodeling effects of teriparatide and alendronate in increasing bone mass. Arch Intern Med 165:1762–1768
34. Black DM, Greenspan SL, Ensrud KE et al (2003) The effects of parathyroid hormone and alendronate alone or in combination in postmenopausal osteoporosis. N Engl J Med 349:1207–1215

35. Dougherty G, Newman D (1999) Measurement of thickness and density of thin structures by computed tomography: a simulation study. Med Phys 26:1341–1348
36. Prevrhal S, Engelke K, Kalender WA (1999) Accuracy limits for the determination of cortical width and density: the influence of object size and CT imaging parameters. Phys Med Biol 44:751–764
37. Boivin GY, Chavassieux PM, Santora AC et al (2000) Alendronate increases bone strength by increasing the mean degree of mineralization of bone tissue in osteoporotic women. Bone 27:687–694
38. Roschger P, Rinnerthaler S, Yates J et al (2001) Alendronate increases degree and uniformity of mineralization in cancellous bone and decreases the porosity in cortical bone of osteoporotic women. Bone 29:185–191
39. Cummings SR, Karpf DB, Harris F et al (2002) Improvement in spine bone density and reduction in risk of vertebral fractures during treatment with antiresorptive drugs. Am J Med 112:281–289
40. McNamara LM, Prendergast PJ (2007) Bone remodelling algorithms incorporating both strain and microdamage stimuli. J Biomech 40:1381–1391
41. Balena R, Toolan BC, Shea M et al (1993) The effects of 2-year treatment with the aminobisphosphonate alendronate on bone metabolism, bone histomorphometry, and bone strength in ovariectomized nonhuman primates. J Clin Invest 92:2577–2586
42. Fischer KJ, Vikoren TH, Ney S et al (2006) Mechanical evaluation of bone samples following alendronate therapy in healthy male dogs. J Biomed Mater Res B Appl Biomater 76:143–148

Bone 45 (2009) 226–231

Contents lists available at ScienceDirect

Bone

journal homepage: www.elsevier.com/locate/bone

Prediction of proximal femur strength using a CT-based nonlinear finite element method: Differences in predicted fracture load and site with changing load and boundary conditions

Masahiko Bessho, Isao Ohnishi *, Takuya Matsumoto, Satoru Ohashi, Juntaro Matsuyama, Kenji Tobita, Masako Kaneko, Kozo Nakamura

Department of Orthopaedic Surgery, Faculty of Medicine, University of Tokyo, 7-3-1 Hongo, Bunkyo-ku, Tokyo 113-0033, Japan

ARTICLE INFO

Article history:
Received 12 June 2008
Revised 6 December 2008
Accepted 16 April 2009
Available online 3 May 2009

Edited by: J. Kanis

Keywords:
Osteoporosis
Hip fracture
Finite element method
CT
Bone strength

ABSTRACT

The annual occurrence of hip fracture due to osteoporosis as of 2002 had reached 120,000 in Japan. The increase has been very rapid. From a biomechanical perspective, hip fractures are thought to be caused in real settings by different directions of loading. Thus, clarification of the loading directions under which the proximal femur is most vulnerable to fracture would be helpful for elucidating fracture mechanics and establishing preventive interventions. The purpose of the current study was to clarify the influence of loading direction on strength and fracture site of the proximal femur using the CT-based nonlinear FE method to determine loading directions under which the proximal femur is most vulnerable to fracture. Contralateral femora were analyzed in 42 women with hip fracture (mean age, 82.4 years), comprising 20 neck fractures and 22 trochanteric fractures. Within 1 week after fracture, quantitative CT of the contralateral femur was performed in each patient and 3-dimensional FE models were created. One stance loading configuration (SC) and four different fall loading configurations (FC) were assigned. Nonlinear FE analysis was performed. Differences in fracture loads depending on differences in loading direction were analyzed and correlations among fracture loads in different loading directions were assessed. Next, fracture sites were also analyzed. Mean predicted fracture load in the SC was 3150 N. Mean fracture loads were 2270 N in FC1, 1060 N in FC2, 980 N in FC3, and 710 N in FC4. The correlation between predicted fracture loads in SC and those in each FC was significant with a correlation coefficient of 0.467–0.631. Predicted fracture sites in the SC appeared at the subcapital region in all patients and were categorized as neck fracture. However, trochanteric fractures occurred in all fall configurations except FC1. In FC1, a significant correlation was seen between real fracture type and predicted type. The current investigation could contribute to the acquisition of useful knowledge allowing the establishment of more efficacious means of preventing hip fractures.

© 2009 Elsevier Inc. All rights reserved.

Introduction

The annual occurrence of hip fracture due to osteoporosis as of 2002 had reached 120,000 in Japan. In Japan, the increase has been very rapid, with a 1.7-fold increase from 1987 to 1992 and a 2.2-fold increase from 1987 to 2002 [1]. More than 90% of fractures were reportedly caused by falls from standing height [2,3]. However, some cases display no clear evidence of falls or trauma [3,4]. From a biomechanical perspective, hip fractures are thought to be caused in real settings by different directions of loading. Thus, clarification of the loading directions under which the proximal femur is most vulnerable to fracture would be helpful for elucidating fracture mechanics and establishing preventive interventions.

Pinilla et al. [5] and Fujii [6] investigated the influence of loading direction on fracture load of the proximal femur. The results of these studies were derived by conducting compression testing of proximal femoral specimens obtained from excised cadaveric femora. One limitation of these studies was that only one load direction could be tested on one specimen and no other direction could be tested using the same specimen. To address this limitation, Ford et al. [7] and Keyak et al. [8] reported simulation studies on the influence of load direction using a computed tomography (CT)-based finite element (FE) method. However, those studies investigated strength of the excised femora and the analytical method was limited to a linear FE method. In addition, none of these studies examined fracture sites in detail. We have established our own CT-based nonlinear FE method to accurately predict fracture load and site on the proximal femur [9].

The purpose of the current study was to clarify the influence of loading direction on strength and fracture site of the proximal femur using the CT-based nonlinear FE method to determine loading directions under which the proximal femur is most vulnerable to fracture. In this study, validity of the FE method was also evaluated by analyzing strength and fracture site of the contralateral femur in

* Corresponding author. Fax: +81 3 3818 4082.
E-mail address: OHNISHII-DIS@h.u-tokyo.ac.jp (I. Ohnishi).

8756-3282/$ – see front matter © 2009 Elsevier Inc. All rights reserved.
doi:10.1016/j.bone.2009.04.241

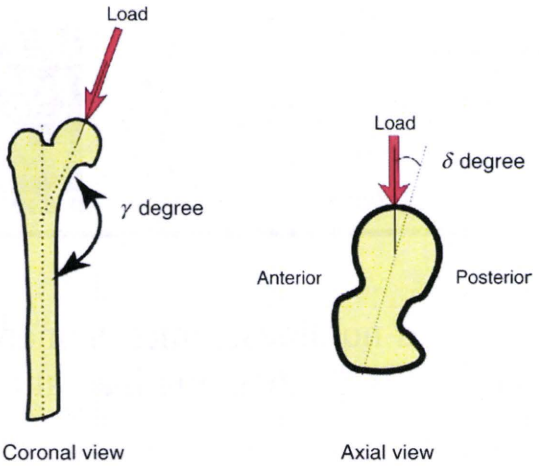

Fig. 1. Definition of the loading direction. Loading direction was defined as the angle γ with reference to the long axis of the femur in the frontal plane and δ with reference to the femoral neck axis in the horizontal plane. Left: coronal plane, right: axial plane.

patients with hip fracture, through which we examined whether our FE method could create fracture in the contralateral femur identical to the real fracture in the patient.

Patients and methods

Contralateral femora were analyzed in 42 women with hip fracture (mean age, 82.4 years; range, 70–92 years; mean height: 146 cm; mean weight: 44 kg), comprising 20 neck fractures (mean age, 81.9 years; mean height: 147 cm; mean weight: 45 kg) and 22 trochanteric fractures (mean age, 82.9 years; mean height: 146 cm; mean weight: 44 kg). No significant differences were seen in mean age ($p=0.60$), height ($p=0.68$) or weight ($p=0.72$). Fifty-three female patients with hip fracture were admitted to the University of Tokyo Hospital between January 2006 and December 2006. These included 4 patients with high-energy injury, 1 with a previous history of cancer, 3 who had received treatment with glucocorticoids, and 3 with metallic implants within the CT scan area. Therefore, after excluding these 11 patients, 42 patients were included in the present study. All patients had sustained fracture by a fall from standing height. All of them approved this study protocol after providing informed consent (initially verbal, later confirmed in writing). With the approval of the ethics committee in our hospital, all the following procedures were performed. Within 1 week after fracture, quantitative CT of the contralateral femur was performed in each patient and 3-dimensional FE models were created. Femora underwent CT using a calibration phantom and a slice thickness of 3 mm from the femoral head to the 17 cm below the minor trochanter (Aquilion Super 4; Toshiba Medical Systems, Japan; 120 kV, 75 mAs, pixel space, 0.625 mm; 512×512 matrix). From the CT data, FE models were created using triangular shell elements with a thickness of 0.4 mm and a size of 3 mm for the outer surface of the cortical bone and tetrahedral solid elements with a size of 3 mm for the rest of the bone [9]. The mean number of solid elements was 80,850, while the mean number of shell elements was 4794. To allow for bone heterogeneity, mechanical properties of each element were computed from the Hounsfield unit value. Ash density was approximated as equivalent to hydroxyapatite density, which neglects the effect of fat content on the Hounsfield unit value for trabecular bone [10–12]. Ash density for each voxel was determined from the linear regression equation derived by relating the Hounsfield unit of a calibration phantom to the equivalent ash density. Bone density of an element was determined from the mean number of Hounsfield units obtained for a total of 17 points in the element [9]. Young's modulus and yield stress of each tetrahedral element were calculated using the equations proposed by Keyak et al. [13] and Keller [14]. Poisson's ratio for each element was set as 0.4 [13]. In previous studies, Young's modulus of the cortex has been found to range from 11 to 24 GPa [15] or from 9 to 21 GPa [16]. Young's modulus of each triangular shell element was set as equivalent to that of the adjacent tetrahedral element located underneath the shell element, while the minimum Young's modulus of the shell element was set as 10 GPa.

Nonlinear FE analysis was performed using the Newton–Raphson method. To allow for the nonlinear phase, mechanical properties of

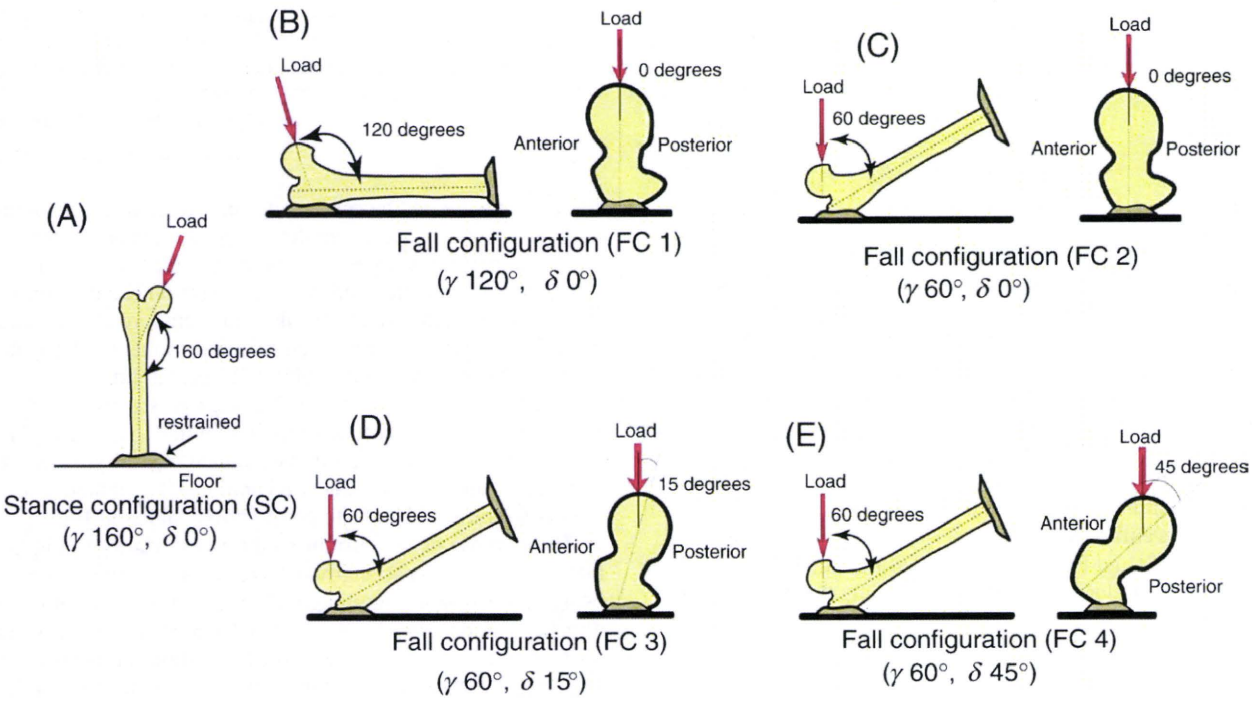

Fig. 2. Loading and boundary conditions. (A) Stance configuration. (B) Fall configuration 1 (FC1). (C) Fall configuration 2 (FC2). (D) Fall configuration 3 (FC3). (E) Fall configuration 4 (FC4).

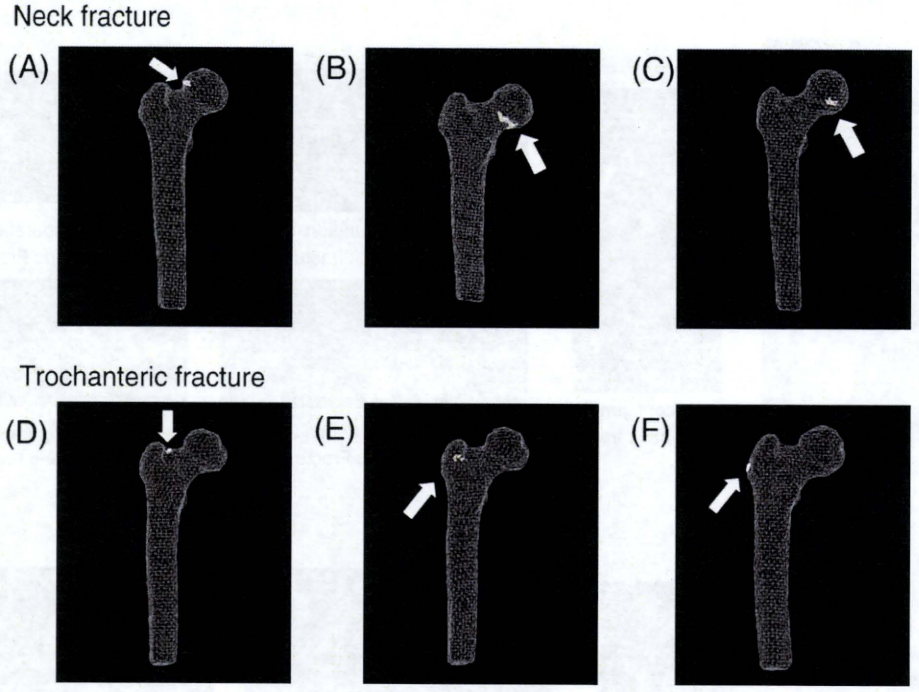

Fig. 3. Fracture types corresponding to each of the predicted fracture sites. Arrow: Predicted fracture site. (A) (B) (C) With predicted fracture sites located at the subcapital region, the type was classified as neck fracture. (D) With predicted fracture sites at the base of the femoral neck, the type was classified as trochanteric. (E) (F) With predicted fracture sites on the trochanteric region, the type was classified as trochanteric.

the elements were assumed to be bi-linear elastoplastic, and the post-yield modulus was set as 5% of E (where E is the pre-yield Young's modulus). The ratio of element ultimate stress to yield stress was assigned as 0.8. The element crack in tension was defined as occurring when maximum principal stress exceeded element ultimate stress. However, we introduced both yield and failure in compression. Yield in compression was defined as occurring when Drucker–Prager equivalent stress exceeded element yield stress. Element failure in compression was then defined as occurring when the negative value of maximum principal strain exceeded 10,000 microstrain. Fracture load was defined as the load when ≥1 shell element failed [9].

Loading direction was defined as the angle γ with reference to the long axis of the femur in the frontal plane and δ with reference to the femoral neck axis in the horizontal plane (Fig. 1) [8]. Angles $\gamma=160°$ and $\delta=0°$ were assigned as stance configuration (SC). For fall loading configuration, four different loading configurations were assigned. Fall configuration (FC) 1 used $\gamma=120°$ and $\delta=0°$. FC2 used $\gamma=60°$ and $\delta=0°$. FC3 used $\gamma=60°$ and $\delta=15°$. Likewise, FC4 used $\gamma=60°$ and $\delta=45°$ (Fig. 2) [6–8].

Differences in fracture loads depending on differences in loading direction were analyzed and correlations among fracture loads in different loading directions were assessed. Next, fracture sites were also analyzed. The predicted fracture type in the FE method was defined as follows. When initial failure of the triangular shell element occurred at a subcapital region, neck fracture was defined. Likewise, if initial failure of the shell element appeared at the basal neck or trochanteric region, trochanteric fracture was defined. The fracture types corresponding to the predicted fracture sites are shown in Fig. 3. Predicted fracture types were compared to the real fracture of the contralateral side in each patient.

Statistical analyses were performed using Pearson's test, Fisher's exact test and Friedman test. Scheffe's test was also utilized for post hoc testing. Values of $p<0.05$ were considered statistically significant.

Results

Mean (±standard deviation (SD)) predicted fracture load in the SC was 3150±611 N. Mean fracture loads were 2270±600 N in FC1, 1060±248 N in FC2, 980±229 N in FC3, and 710±174 N in FC4 (Fig. 4). Mean predicted fracture load was significantly larger than in the SC than in all FCs except FC1 ($p<0.001$). To compare mean fracture loads among FCs, the load in FC1 was significantly larger than those of FC2, FC3 and FC4 ($p<0.01$, $p<0.001$, $p<0.001$,

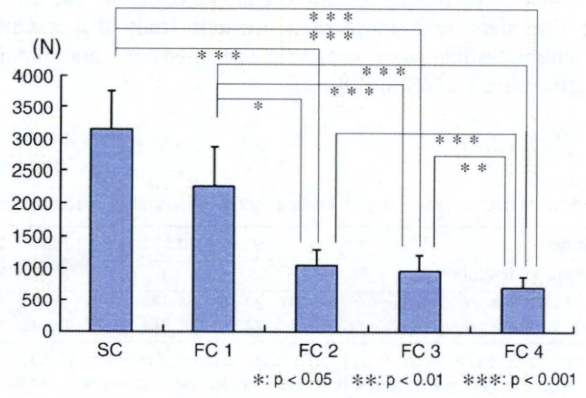

Fig. 4. The mean predicted fracture loads for each configuration. The *X* axis indicates load and boundary conditions and the *Y* axis indicates predicted strength. SC: Stance configuration, FC: fall configuration.

Table 1
Correlations (r) of the predicted fracture loads for each loading configuration.

	SC	FC1	FC2	FC3	FC4
SC	–	0.467**	0.615***	0.614***	0.631***
FC1	0.467**	–	0.586***	0.584***	0.463**
FC2	0.615***	0.586***	–	0.894***	0.728***
FC3	0.614***	0.584***	0.894***	–	0.861***
FC4	0.631***	0.463**	0.728***	0.861***	–

** $p<0.01$.
*** $p<0.001$.

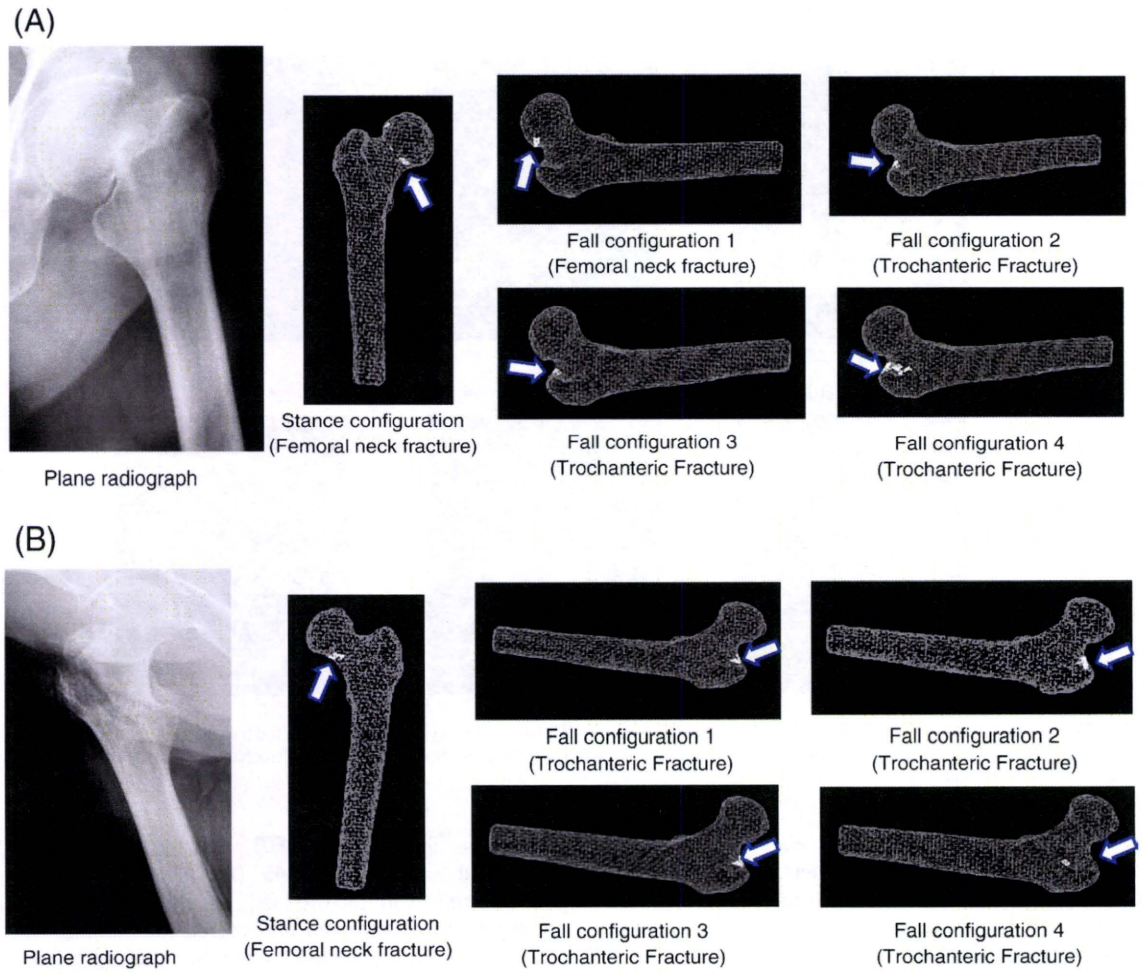

Fig. 5. The predicted fracture sites for each configuration. The shell elements in failure are shown on the 3 dimensional finite element model. Arrow: The predicted fracture site. Words in parentheses: the predicted fracture type. (A) 89 years old (femoral neck fracture, Garden classification, Stage IV) (B) 83 years old (trochanteric fracture, Evans classification Type I, group 2).

respectively). Load was significantly larger in FC2 than in FC4 ($p<0.001$). Likewise, load was significantly larger in FC3 than in FC4 ($p<0.01$).

Correlation coefficients of predicted fracture load among all configurations are listed in Table 1. The correlation coefficient relating the predicted strength under SC to that under FC1 was 0.467 (95% confidence interval: 0.190–0.675, $p=0.0016$). The coefficient relating SC to FC2 was 0.615 (95% confidence interval: 0.383–0.775, $p<0.0001$). The coefficient relating SC to FC3 was $r=0.615$ (95% confidence interval: 0.383–0.775, $p<0.0001$). The coefficient relating SC to FC4 was $r=0.631$ (95% confidence interval: 0.405–0.785, $p<0.0001$). The coefficient relating FC1 to FC2 was $r=0.586$ (95% confidence interval: 0.344–0.756, $p<0.0001$). The coefficient relating FC1 to FC3 was $r=0.584$ (95% confidence interval: 0.340–0.754, $p<0.0001$). The coefficient relating FC1 to FC4 was $r=0.463$ (95% confidence interval: 0.185–0.672, $p=0.0017$). The coefficient relating FC2 to FC3 was $r=0.894$ (95% confidence interval: 0.810–0.942, $p<0.0001$). The coefficient relating FC2 to FC4 was $r=0.728$ (95% confidence interval: 0.545–0.845, $p<0.0001$). The coefficient relating FC3 to FC4 was $r=0.861$ (95% confidence interval: 0.755–0.923, $p<0.0001$).

All predicted fracture sites could be categorized by the failure of shell elements into two types, namely neck fractures and trochanteric fractures (Fig. 5). Predicted fracture sites in the SC appeared in the subcapital region in all patients and were categorized as neck fractures. However, trochanteric fractures occurred in all fall configurations except FC1. In FC1, both the neck and trochanteric fractures occurred, with 16 neck fractures in 20 patients with contralateral neck fracture and 18 trochanteric fractures in 22 patients with contralateral trochanteric fractures. A significant correlation was seen between real fracture type and predicted type ($p<0.001$) (Table 2).

Discussion

From the results of our study, the predicted strength under the loading condition simulating a fall in the posterolateral direction was smaller than that by a fall in the lateral direction. These results were consistent with those of a previous study that conducted mechanical testing using cadaveric specimens [6] and predicted strength using a CT/FEM [7,8].

Table 2
The predicted fracture types for each loading configuration and each fracture type.

Conditions	SC		FC1		FC2		FC3		FC4	
The predicted fracture type	N	T	N	T	N	T	N	T	N	T
Patients with femoral neck fracture ($n=20$)	20	0	16	4	0	20	0	20	0	20
Patients with trochanteric fracture ($n=22$)	22	0	4	18	0	22	0	22	0	22

Predicted fracture sites in the SC appeared in the subcapital region in all patients and were categorized as neck fractures. However, trochanteric fractures occurred in all fall configurations except FC1. In FC1, both the neck and trochanteric fractures occurred, with 16 neck fractures in 20 patients with contralateral neck fracture and 18 trochanteric fractures in 22 patients with contralateral trochanteric fractures. N: femoral neck fracture, T: trochanteric fracture.